



Call: H2020-SC5-2014-two-stage

Topic: SC5-01-2014

**PRIMAVERA**

Grant Agreement 641727



**PRocess-based climate sIMulation: AdVances in high resolution modelling and  
European climate Risk Assessment**

### **Deliverable D3.3**

***Quantification of the effect of improved sea ice processes***

Deliverable Title	<i>Quantification of the effect of improved sea ice processes</i>		
Brief Description	<i>Quantification of the effect of improved sea ice processes on representing Arctic sea ice and the impact on European climate and robustness across multi-model resolution ensemble</i>		
WP number	3		
Lead Beneficiary	CMCC		
Contributors	<p><i>Louis-Philippe Caron, BSC</i>  <i>Eduardo Moreno-Chamarro, BSC</i>  <i>Doroteaciro Iovino, CMCC</i>  <i>Pier Giuseppe Fogli, CMCC</i>  <i>Sarah Keeley, ECMWF</i>  <i>Retish Senan, ECMWF</i>  <i>Ann Keen, Met Office</i>  <i>Ed Blockley, Met Office</i>  <i>Klaus Wyser, SMHI</i>  <i>Wang Shiyu, SMHI</i>  <i>Torben Koenigk, SMHI</i>  <i>David Docquier, UCLouvain</i>  <i>Jean Sterlin, UCLouvain</i>  <i>François Massonet, UCLouvain</i>  <i>Thierry Fichefet, UCLouvain</i></p>		
Creation Date			
Version Number			
Version Date			
Deliverable Due Date			
Actual Delivery Date			
Nature of the Deliverable		<p><i>R – Report</i></p> <p><i>P – Prototype</i></p> <p><i>D – Demonstrator</i></p> <p><i>O – Other</i></p>	
Dissemination Level/ Audience		<p><i>PU – Public</i></p> <p><i>PP – Restricted to other programme participants, including the Commission services</i></p>	
		<p><i>RE – Restricted to a group specified by the consortium, including the Commission services</i></p>	
		<p><i>CO – Confidential, only for members of the consortium, including the Commission services</i></p>	

<b>Version</b>	<b>Date</b>	<b>Modified by</b>	<b>Comments</b>
Version 1	18/2/2019	Doroteaciro lovino	Contributions on sea ice properties from every partner
Version 2	25/2/2019	Doroteaciro lovino	Updated plots and texts
Version 3	28/2/2019	Doroteaciro lovino	Final version

**Table of Contents**

1. Executive Summary.....	5
2. Project Objectives.....	6
3. Detailed Report.....	7
3.1 <i>Description of model developments</i> .....	7
3.2 <i>Results: Arctic sea ice properties</i> .....	9
3.2.1 Ice thickness distribution .....	9
3.2.2 Melt pond schemes .....	18
3.2.3 Rheology .....	30
3.3 <i>Impact on European climate</i> .....	38
4. Lessons Learnt.....	45
5. Links Built.....	45

## **1. Executive Summary**

The focus of this deliverable is to quantify the impact of the improved representations of key processes on the representation of Arctic sea ice in the sea ice component of a set of climate models. The consensus among models remains elusive on the magnitude and spatial patterns of Arctic sea ice loss or on when ice-free Arctic conditions will be reached. Hence, in order to better simulate the observed sea ice behaviour and mainly to advance our understanding of the predictability of sea ice conditions, improved representation of key sea ice processes are necessary.

WP3c developed and implemented new physical parameterisations specifically designed for use in combination with high spatial resolution. The study focused on the improvements of two sea ice models, both widely used for climate study, namely LIM (see Fichefet et al., 1997 for LIM2 and Rousset et al., 2015 for LIM3) and CICE (Hunke and Lipscomb, 2010). Improvements have been tested in more than one model wherever possible, in order to improve robustness.

Sea ice dynamics and thermodynamics (such as rheology, multi-category ice), as well as surface schemes (such as melt pond parameterizations) have been improved, aiming also to improve the representation of heat fluxes at the atmospheric-sea ice interface, and potentially affecting heat exchanges at the ocean-sea ice interface. The response of Arctic sea ice variability to new physics have been analysed.

New parameterizations have been incorporated into in global models at standard (~100 km scale) and enhanced resolution (~25 km scale) with the final scope to investigate their impact on the regional climate of Europe. Changes have been validated within the forced ocean-sea ice models, and then in coupled model context of present day and the recent past through comparison with available observational-based data sets and satellite products.

The model developments and sensitivity experiments carried out in this sub WP provide the possibility to re-formulate and re-assess models for the Stream 2 simulations. Our results provide indications on how different modelling strategies are beneficial to the simulation of key processes and how they can contribute to governing European climate variability and change. The improved sea ice components, that incorporate the new developments from WP3, have been already inserted in the climate models of the WP partners and will feed, at least partially, into the Stream 2 set of experiments that will be performed in WP6, with the goal of delivering improved modelling capability for the Europe region.

While results do generally show a significant advancement of the sea ice components, it is worth mentioning that the effect of new sea ice component in simulating the European climate cannot be completely analyzed in relation to one single development in one single code, but requires a wider range of results from a multi-model effort. Moreover, the effect on climate does largely depend on the ocean and atmospheric components of the climate system, and their spatial resolutions. In other words, the improved sea ice models delivered by WP3 can lead to the improvement of a specific process in a specific model, while they do not necessarily improve other aspects of sea ice or climate. The partners involved in this sub-WP do not share the same numerical tools, and the simulations run to test the new physics all cover recent decades, but are relatively short for climate assessment.

This deliverable motivates and describes the implemented new schemes in Section 3.1. The main results are detailed in Section 3.2 and 3.3. The lesson coming from the work undertaken is presented in Section 4, and links with other WPs and projects are summarized in Section 5.

## **2. Project Objectives**

With this deliverable, the project has contributed to the achievement of the following objectives (DOA, Part B Section 1.1) WP numbers are in brackets:

No.	Objective	Yes	No
A	To develop a new generation of global high-resolution climate models. (3, 4, 6)		
B	To develop new strategies and tools for evaluating global high-resolution climate models at a process level, and for quantifying the uncertainties in the predictions of regional climate. (1, 2, 5, 9, 10)		
C	To provide new high-resolution protocols and flagship simulations for the World Climate Research Programme (WCRP)'s Coupled Model Intercomparison Project (CMIP6) project, to inform the Intergovernmental Panel on Climate Change (IPCC) assessments and in support of emerging Climate Services. (4, 6, 9)		
D	To explore the scientific and technological frontiers of capability in global climate modelling to provide guidance for the development of future generations of prediction systems, global climate and Earth System models (informing post-CMIP6 and beyond). (3, 4)		
E	To advance understanding of past and future, natural and anthropogenic, drivers of variability and changes in European climate, including high impact events, by exploiting new capabilities in high-resolution global climate modelling. (1, 2, 5)		
F	To produce new, more robust and trustworthy projections of European climate for the next few decades based on improved global models and advances in process understanding. (2, 3, 5, 6, 10)		
G	To engage with targeted end-user groups in key European economic sectors to strengthen their competitiveness, growth, resilience and ability by exploiting new scientific progress. (10, 11)		
H	To establish cooperation between science and policy actions at European and international level, to support the development of effective climate change policies, optimize public decision making and increase capability to manage climate risks. (5, 8, 10)		

### 3. Detailed Report

#### 3.1 Description of model developments

##### ***Ice Thickness Distribution***

The Ice Thickness Distribution (ITD) is a core component of modern sea ice models, it accounts for the unresolved spatial variability of sea ice thickness within each model grid cell. In the current version of LIM3, the model ITD numerical formulation follows Lipscomb (2001), and is discretized into a fixed number of categories, each of which occupies a different grid areal fraction and constrain the ice to remain between user-prescribed boundaries. In its current version, LIM's default ITD discretization uses a fitting function that sets category boundaries between 0 and  $3h$ , with the expected mean sea ice thickness over the domain and with a finer resolution for the thin ice (Rousset et al., 2015). The upper and lower ice thickness limits of categories  $i = 1, \dots, N$  are  $f(i-1)$  and  $f(i)$  with:

$$f(i) = \left( \frac{N(3\underline{h}+1)^{\alpha}}{(N-i)(3\underline{h}+1)^{\alpha}+i} \right)^{\alpha^{-1}} - 1 \quad (1)$$

where  $N$  is the number of categories,  $\alpha=0.05$  and  $i$  is the category index. The upper limit of the last category is always reset as  $3h$ , up to 99 m, to allow hosting very thick ice.

We run three sets of sensitivity simulations with different ITD configurations (shown in Figure 1). The ITD presents two features: the number of categories and their boundaries' positions. In the first configuration, only the number of categories is modified and both the number and position of the categories change following the default-parameterization algorithm in LIM3 according to Equation 1. In the second configuration, the resolution of the distribution is unchanged; instead new thickness categories are successively appended for the thickest ice. In the third configuration, the lower boundary of the last category is locked to 4 m (which is about the maximum thickness that thermodynamic ice growth can sustain in the Arctic) and each category is successively split into two, which particularly impacts the thinnest ice categories.

##### ***Melt ponds in LIM3 and CICE (forced and coupled mode)***

Melt ponds play an increasingly important role in the context of the current melting of the Arctic ice cover and their incorporation in the sea ice component of climate models is essential for accurate representation of future sea ice variability. There are several schemes for modelling the ponds that form on the surface of melting sea ice.

Melt ponds have been tested in two different sea ice models, LIM3 (Rousset et al., 2015) and the CMCC version of CICE (based on CICE4, Hunke and Lipscomb, 2010). In both cases, the sea ice components have been tested coupled to NEMOv3.6 ocean component (forced by atmospheric reanalysis) and in coupled mode (in EC-Earth and CMCC-CM, respectively).

In LIM3, we considered three melt-pond parameterizations from an implicit scheme toward a more detailed modeling of melt pond physics. The three melt-pond methods are:

- a prescribed parameterization, in which two constant parameters (melt-pond fraction and depth) are prescribed;
- an empirical parameterization, in which a fraction of the melt water accumulates in pond reservoirs; the volume in the ponds is cleared when the ice thickness is below 0.1m, or

released exponentially when the surface freezes; this parameterization is based on Holland et al. (2012);

- a topographic parameterization, in which melt-pond evolution is computed from the ice topography as inferred from the ice-thickness distribution, based on Flocco and Feltham (2007) and Flocco et al. (2010).

Improving the CMCC-CICE ice model, we focused on two melt pond parameterizations. In the first set of experiments, the CESM option of melt pond formulation was set. In this simple parameterization of surface melt pond, designed to be used together with the Delta-Eddington shortwave scheme, melt pond volume is carried on each ice thickness category as an area tracer. Defined as the product of pond area and depth, the melt pond volume grows through addition of ice or snow melt-water or rainwater, and shrinks when the ice surface temperature becomes cold. All melt water runs off into the ocean. For a second set of runs, we have implemented a topographic formulation (TOPO), a more complex melt pond thermodynamics following Flocco et al. (2012). In this scheme, also used in conjunction with the Delta-Eddington radiation scheme (ponded ice albedo are not prescribed but calculated from inherent optical properties), ice thickness distribution approximates the effects of topography on melt pond evolution. Melt water runs downhill and accumulates on the thinnest ice categories first, saturating remaining snow, with an imposed maximum fractional coverage that depends linearly on ice thickness. As the melting season progresses, the sea ice beneath the melt water becomes more porous owing to a reduction in solid fraction. Ponds drain vertically through sea ice when it is permeable, and refreeze when the surface energy balance is negative. Pond area and thickness are carried as separate tracers.

#### ***An anisotropic sea ice rheology (in the GC3.1 configuration of the HadGEM3 model)***

Most modern climate models use a continuum model for the sea ice dynamics, where it is assumed that model grid cells are large enough to contain a representative sample of ice types, with a sufficiently large number of leads and ridges for there to be no preferred orientation. In such a situation, it is acceptable to use an isotropic model, such as the elastic-viscous-plastic (EVP) rheology used within the sea ice component of HadGEM3 (CICE). However, for models being run at sufficiently fine resolution, grid cells can no longer contain a representative sample of ice type, and the continuum assumption potentially breaks down. The question then arises as to whether isotropic sea ice rheologies like EVP, designed for coarse resolution, are suitable for use with high-resolution climate models. The elastic-anisotropic-plastic (EAP) rheology was developed to explicitly account for the sub-grid scale anisotropy of the sea ice cover (Wilshinsky et al., 2006; Tsamados et al., 2013), which should be more appropriate for high-resolution climate simulations.

The EAP rheology has been included within the GC3.1 configuration of the HadGEM3 model. To reduce the computational cost of using EAP, several efficiency upgrades to the EAP formulation, provided by the Centre for Polar Observation and Modelling (CPOM) – the original developers of the EAP rheology, have also been incorporated into HadGEM3. Although the EAP rheology is more complicated than EVP the computational cost of the whole HadGEM3 coupled model remains broadly similar.

Two 50-year equilibrium climate runs, with constant year-2000 forcing, have been performed using the EAP rheology. This has been done for both the low-resolution (N96-ORCA1) and the high-resolution (N216-ORCA025) HadGEM3 configurations that are being used as the UK's physical climate model contribution to CMIP6. The impact of the EAP rheology is being

quantified by comparison to existing HadGEM3 runs performed with the standard Elastic-Viscous-Plastic (EVP) rheology.

### 3.2 Results: Arctic sea ice properties

#### 3.2.1 Ice thickness distribution

**BSC** and **UCLouvain** explore the impact of different configurations of the sea ice thickness distribution (ITD) on the mean state and variability of the Arctic sea ice. We use simulations with the sea ice model LIM3, coupled to the ocean model NEMO3.6 (NEMO3.6-LIM3), which are both components of the EC-Earth3 climate model. The NEMO3.6-LIM3 model is run on the global ORCA1 grid, which features a nominal horizontal resolution of 1° and 75 vertical levels. It is forced by the DRAKKAR atmospheric Forcing Set version 5.2 (DFS5.2; Dussin et al., 2016) over the period 1979–2014.

Through the ITD, LIM can represent subgrid-scale distribution of sea ice thickness, enthalpy, and salinity (Thorndike et al., 1975).

#### Impact on the simulated mean sea ice state (**UCLouvain**)

The main consequence of using a larger number of ice thickness categories with the default parameterization is an increase in the ice volume in winter (Fig. 2). In the Arctic, the increase persists during the whole seasonal cycle, even though it becomes smaller in summer. To position the volume produced by our model, a comparison is made with the PIOMAS reanalysis (Schweiger et al., 2011). The model produces higher volume than the PIOMAS reanalysis for simulations with more than three categories. In the Antarctic, the increase is limited to the ice-growing season while the rest of the year features a decrease in volume when using only few categories (S1.01 and S1.03), which is due to an excessive sea ice extent in summer. In either hemisphere, the annual maximum of ice volume does not converge to an asymptotic value when increasing the number of categories: even at 100 categories (not shown), the winter ice volume is significantly higher than with 50 categories. Spatially, the thickness response is rather uniform, with maximum values in the Beaufort Sea in the Arctic (not shown).

The origin of volume and thickness increases with the number of ice thickness categories can be explored with the tendency diagnostics provided in LIM. Indeed, variations in state variables, including volume in each category and therefore the aggregate volume, can be attributed to various physical processes accounted for in the model such as open water ice formation, bottom growth, bottom melt, surface melt and snow-ice formation. We find that the increase in sea ice thickness is mainly due to an enhancement of thermodynamic basal growth in winter (Fig. 3). Our hypothesis is that, for the same grid cell average thickness, a better resolved ITD results in larger basal ice growth rates due to the inverse relationship between conductive heat fluxes and sea ice thickness.

Beyond the number of categories, the *position* of the category boundaries can have an influence on the simulated mean state: concentrating 50 categories in the first meter has not the same impact as spreading these 50 categories over a wider thickness range. We determine the minimum requirements that an ITD should have in order to host deformed ice produced by the model, by plotting the thickness distributions in the S2 set of experiments (Figs. 1 and 4). The histograms in Figure 4 display the relative areal abundance of sea ice in

each of the model categories. It can be seen from this figure that the shapes of these distributions do not change substantially beyond the S2.09 and S2.07 experiments for the Arctic and Antarctic, respectively. Since these two experiments have their lowest boundary of the thickest category at 4 and 2 meters, respectively, we conclude that resolving thick categories with these lower bounds is necessary to host deformed ice produced by the model, and therefore to allow sustaining thermodynamic growth in thinner categories.

Based on these results, we recommend to the users of the NEMO3.6-LIM3 the use of the default ITD formulation provided in the code and in the sea ice namelist (five categories with lower bounds at 0.0, 0.45, 1.13, 2.14, 3.67 m). We advise users against using the model with one category (as has been done in the past) since that configuration ignores by definition the sub-grid scale variability of sea ice thickness, which implies an underestimation of heat conduction in fluxes and therefore bottom ice growth (Massonnet et al., in review).

### **K-means clustering analysis of interannual sea ice concentration variability (BSC)**

We further explore the impact of the ITD on the interannual sea ice concentration (SIC) variability in the Arctic. The model simulations are compared with three satellite SIC observational products: HadISSTv2.2 (Titchner and Rayner, 2014), NSIDC [Cavalieri et al., 1996], and OSISAF (EUMETSAT SAF, 2016). For both the simulations and data, we analyze interannual variability in the Arctic sea ice concentration during two seasons, January through March (JFM) and August through October (ASO), for the period 1979-2014. Variability in each season is characterized through three clusters extracted using K-means cluster analysis. Three clusters is the optimal number, as derived from a suite of 10 indices that allow determining the most robust choice of the number of clusters. Observed JFM and ASO clusters are shown in Figures 5 and 6 respectively. Each cluster is characterized by a spatial pattern of sea ice concentration anomalies, the percentage of occurrence over the period 1979-2014, and a time series of cluster occurrence (which indicates which cluster is the closest to the anomaly pattern in a year as well as their Euclidean distance, defined as the root-mean-squared error difference). The leading winter (JFM) cluster resembles the quadrupole that has been described by Close et al. (2017), whereas the third one reflects the NAO imprint on the sea ice concentration, with more sea ice in the Labrador Sea during positive NAO phases (e.g., Bader et al., 2011). The three summer clusters reflect a long-term trend of melting sea ice.

To evaluate the impact of the ITD configuration on the sea ice concentration, the observed and the simulated clusters are spatially correlated (Fig. 7). In winter the impact of the different ITD configuration is small and most simulations capture well the observed cluster of variability; nonetheless, there is a slight drop in the spatial correlation coefficient in the third clusters for a very high number of categories, which appears related to a too-high refinement of the thinnest ice. In summer, the ITD configuration has a slightly bigger impact, especially for the second cluster. It is however difficult to draw any particular conclusions beyond that one category tend to perform the worst.

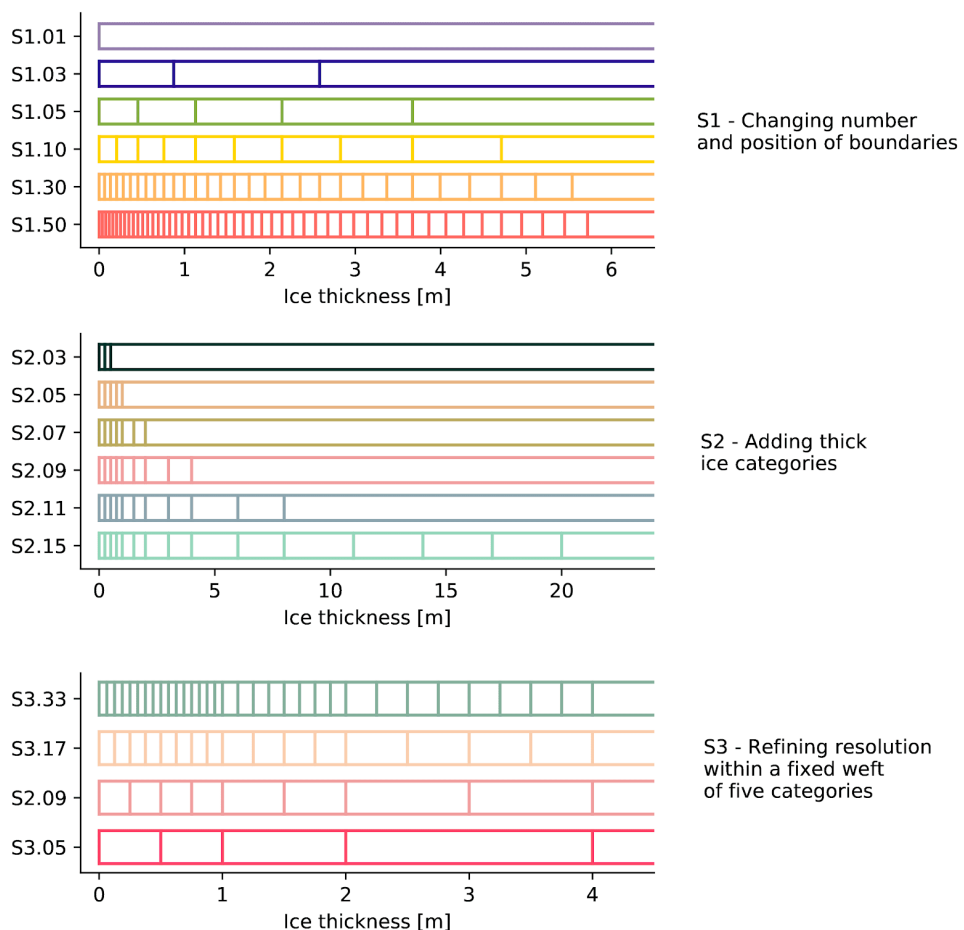


*Figure 1. Ice thickness category boundaries in the three sets of sensitivity experiments. The upper boundary of the last category is always set to 99.0 m. Note that the ice thickness scale is different in the three panels. Because the ITD discretization in the third set of experiments (S3) branches from experiment S2.09 of the second set, that experiment is repeated in the list. From Massonet et al. (in review).*

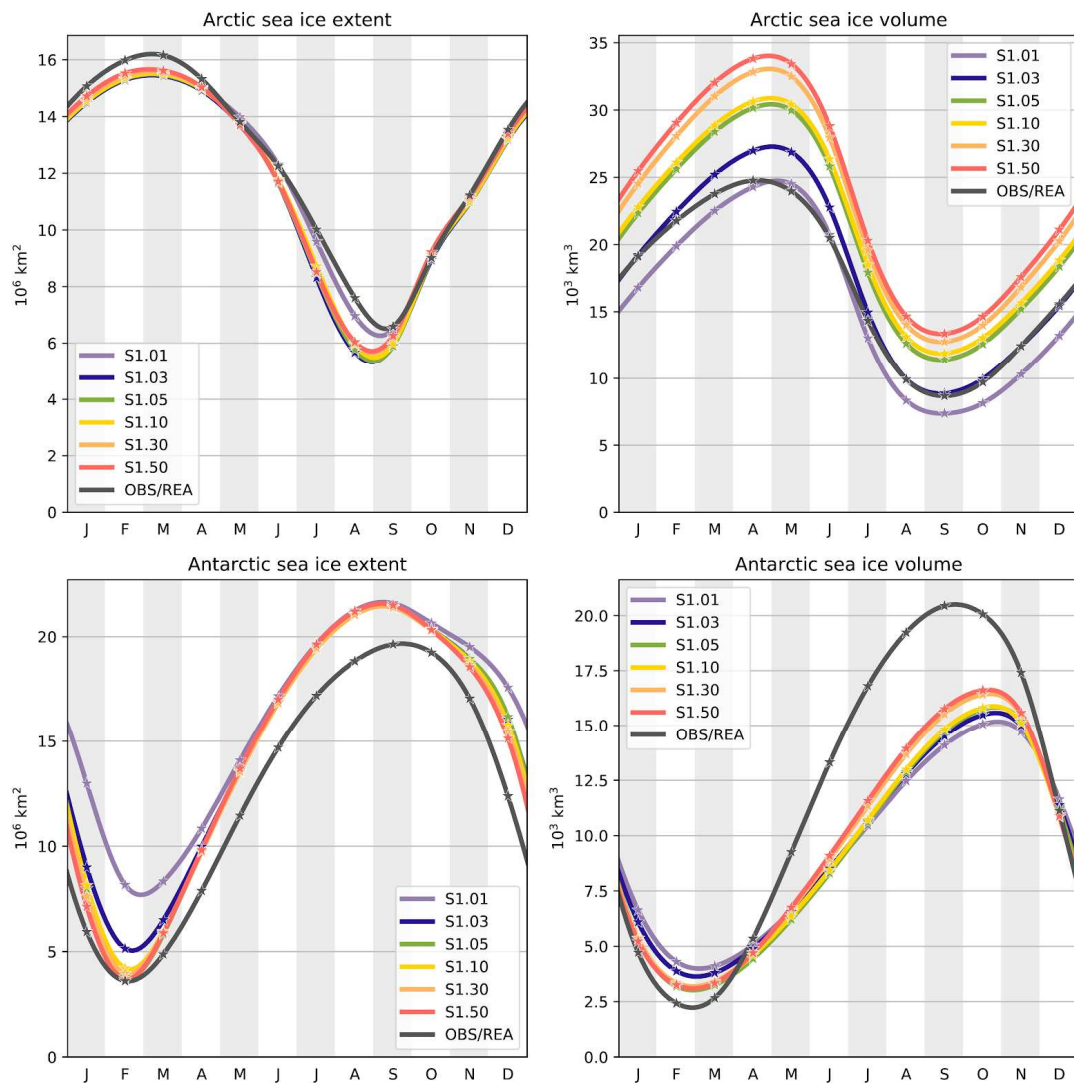


*Figure 2. Mean seasonal cycles of Arctic (top) and Antarctic (bottom) sea ice extents (left) and volumes (right), over 1995-2014, in the first set of sensitivity experiments. Ice extents derived from the OSI SAF sea ice concentration observational product (OSI-409a) (EUMETSAT, 2015) are also shown, as well as Arctic and Antarctic ice volumes derived from the PIOMAS and GIOMAS reanalyses, respectively (Zhang and Rothrock, 2003; Schweiger et al., 2011). The stars show the monthly data and the curves are cubic interpolations between the data points. From Massonnet et al. (in review).*

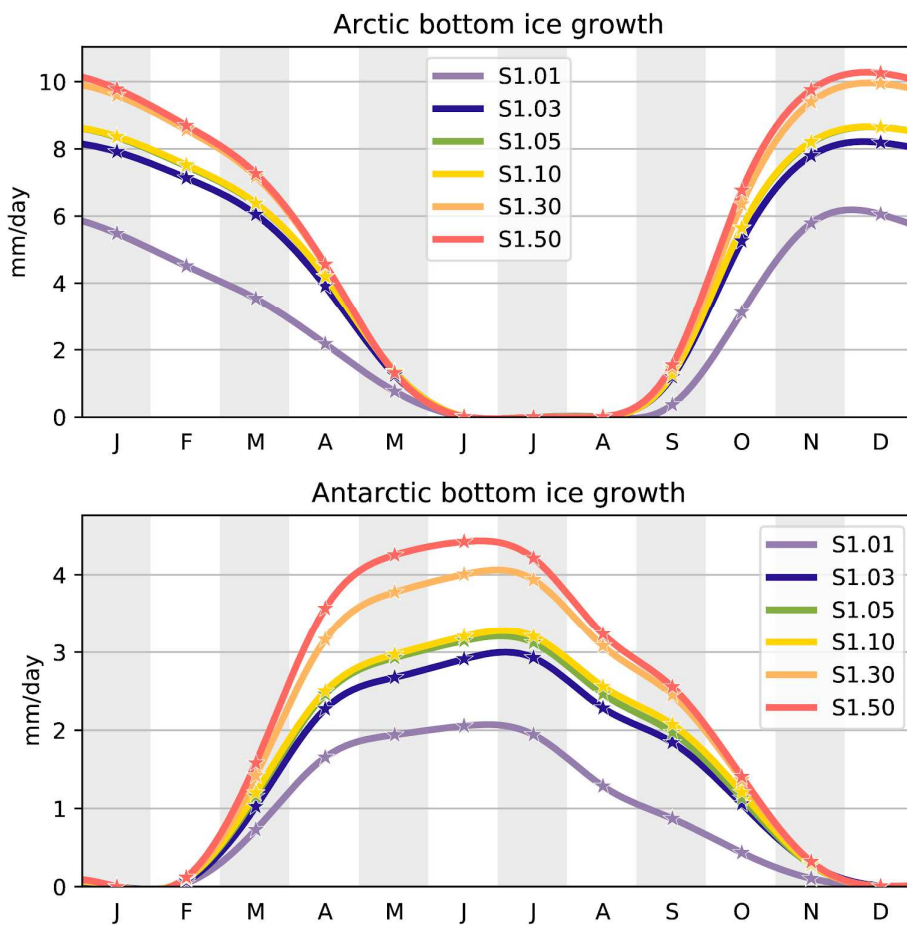


*Figure 3. Mean seasonal cycles of Arctic (top) and Antarctic (bottom) bottom ice growth, over 1995–2014, in the first set of sensitivity experiments. The spatial averages are computed over all grid cells for which the simulated 1995–2014 seasonal cycle of sea ice concentration exceeds 99% year-round. From Massonnet et al. (in review).*

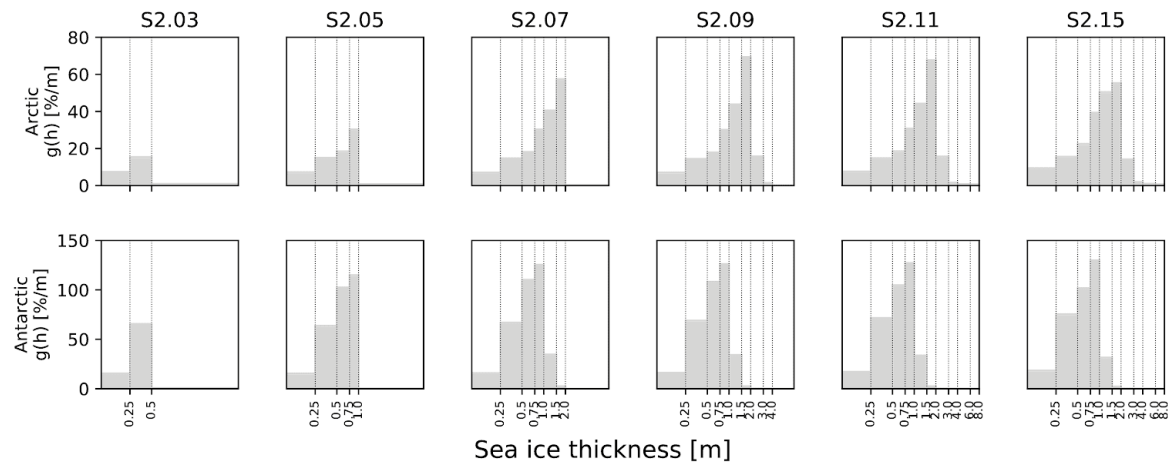


*Figure 4. Mean ice thickness distribution in the second set of sensitivity experiments. For each ice thickness category, the relative areal proportion of ice for that category was estimated from the Arctic (March; top) and Antarctic (September; bottom) 1995–2014 average sea ice concentration. Thin vertical lines delimit the category boundaries. Note that, for the sake of readability, the spacing along the x-axis is logarithmic. The upper bound of the last category is always set to 99 m and is not displayed. From Massonnet et al. (in review).*

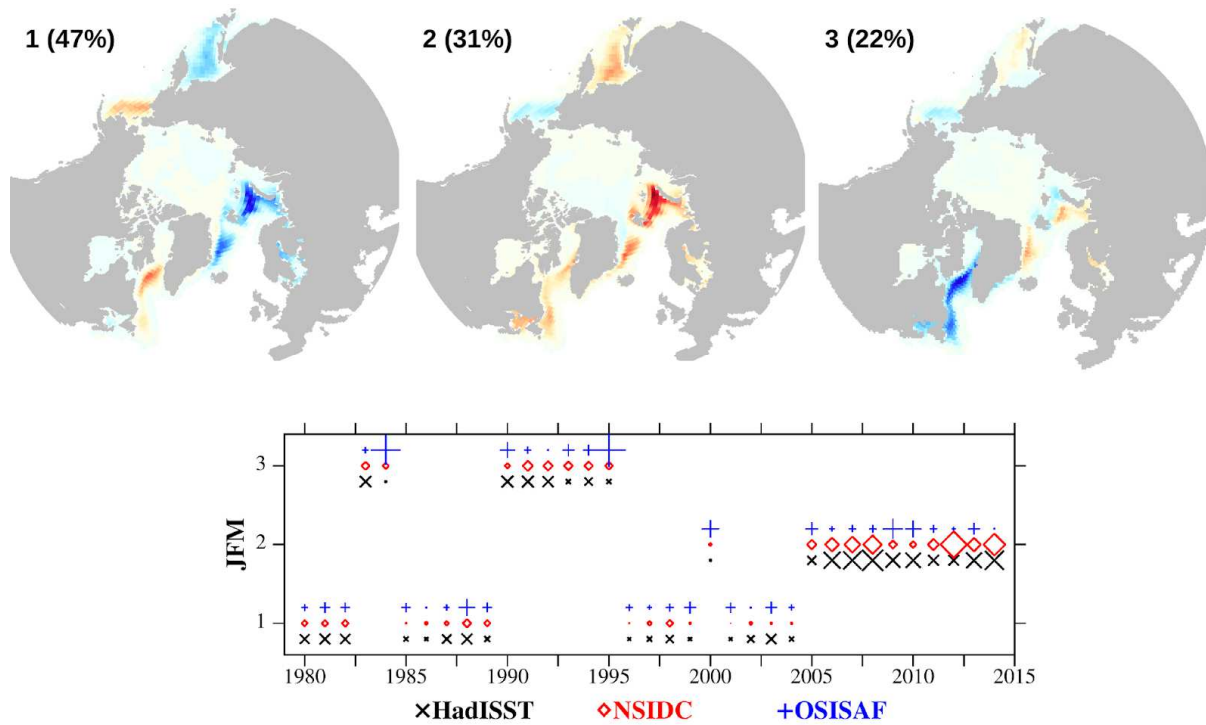


*Figure 5. Top: Winter (JFM) cluster patterns of anomalous sea ice concentration in OSISAF, with their respective percentage of occurrence over the period 1979–2015. Clusters in HadISST and NSIDC are very similar and therefore are not shown here. Bottom: the associated time series of cluster occurrences and the Euclidean distance (RMS difference) between a pattern in a year and the associated cluster, with a larger symbols accounting for larger distances.*

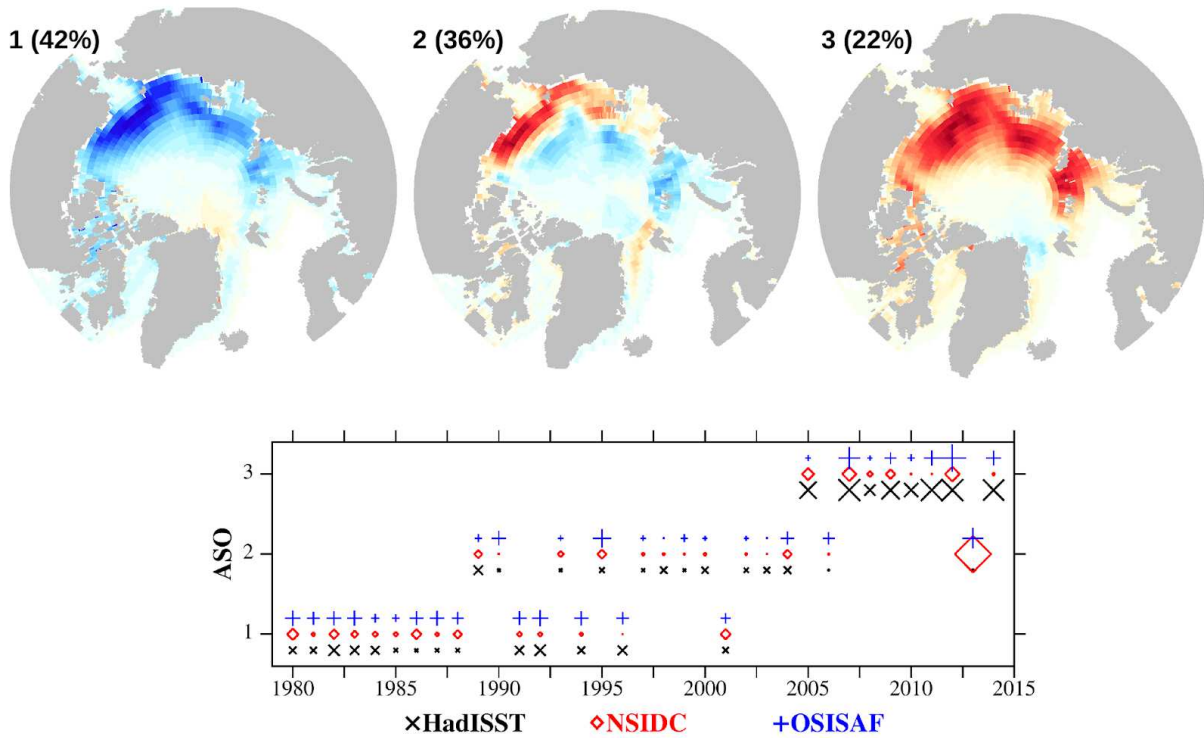


Figure 6. As in Figure 5, but for the clusters in summer (ASO)

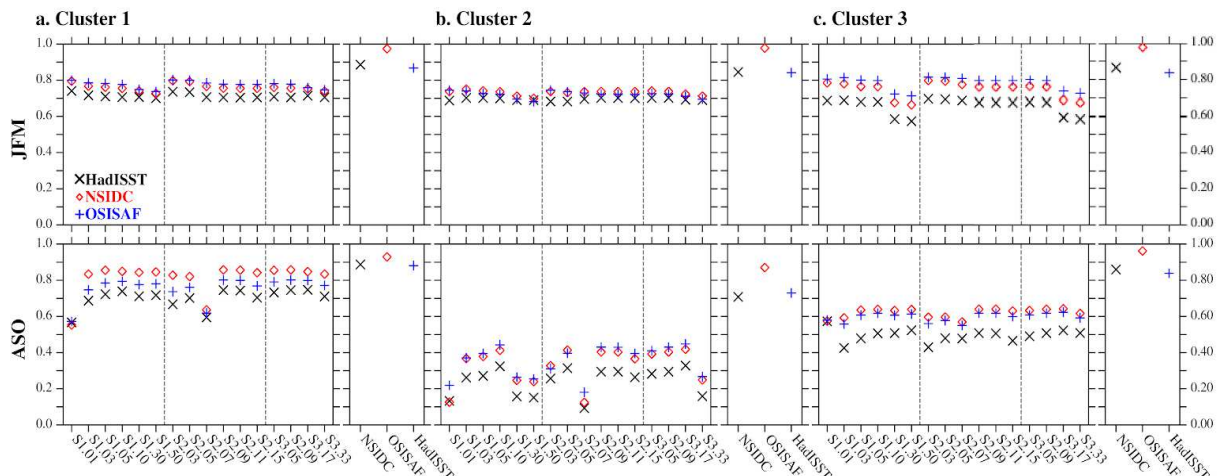


Figure 7. Spatial correlation coefficients between the observed and the simulated clusters in winter (JFM; top) and summer (ASO; bottom). Each different column corresponds to a different experimental set up, as defined in Figure 1. The spatial correlation coefficients between the different observational products for each cluster is also shown.

At ECMWF, the ice model physics was improved by moving from LIM2 to LIM3. The main differences between LIM2 and LIM3 are the prognostic variables, formulation of the ice rheology and number of ice thickness categories. LIM3 has prognostic salinity rather than using a constant value and models the ice thickness distribution, rather than parameterizing it. LIM3 uses an EVP rheology rather than the VP formulation used in LIM2. The default LIM3

configuration has an explicit ITD with 5 ice categories that enables to resolve the more intense growth and melt of thin ice, as well as the redistribution of thinner ice onto thicker ice due to ridging and rafting, while LIM2 is a single-category model. To test the impact of ice thickness distribution alone we run LIM3 with 1 and 5 categories. The single category formulation of LIM3 is close to the setup of LIM2 so the differences are largely down to halo-dynamics that is part of LIM3. For the 5-category LIM3 model, the category boundaries use the expected mean thickness formulation ( $h$ ,  $\alpha$ ) scheme as described in Rousset et al (2015). We find that LIM3 with 5 thickness categories produces the best model climate in terms of sea ice variables and European region climate variables.

We used the ocean component model NEMO3.6 at 0.25-degree resolution with 75 vertical levels (which is not used operationally by ECMWF). Ocean-ice forced runs were carried out for the period 1979-2014 forced with ERA-Interim forcing and provide initial conditions for the coupled runs.

All coupled model runs were made with an atmospheric component model IFS CY45R1 Tco199 (~50 km horizontal resolution) with 91 vertical levels. As analysed initial conditions did not exist for LIM3, we used a forced ocean-ice run to provide an initial state for 1980 for the ocean ice model. Coupled integrations were then performed for 1980-2014. The different ice physics used in the experiments are described in the table:

<i>Experiment name</i>	<i>Ice physics model</i>	<i>Rheology</i>	<i>Number of categories</i>	<i>Category boundaries</i>	<i>Salinity</i>
LIM2	LIM2	VP	1	Monocat scheme	Constant
LIM3-1C	LIM3.6	EVP	1	Monocat scheme	Prognostic
LIM3-5C	LIM3.6	EVP	5	Mean thickness $h(\text{mean})=2$	Prognostic

Results show that the use of LIM3 rather than LIM2 improves the representation of the seasonal cycle (Fig. 8), which is consistent with previous studies (e.g. Massonnet et al., 2011). The forced runs (dashed lines) fit the climatological seasonal cycle better (as expected, no atmospheric model bias). The multicategory runs, show the best representation of the rate of change, i.e. faster melt and freeze, which was a problem with LIM2. In all cases, except the forced single category LIM3, we tend to over predict the extent and volume in winter and this is exacerbated in the coupled runs.

Figure 9 shows the time series for March and September sea ice extent and volume; the dashed lines show the forced runs and the solid lines show the coupled integrations. Biases are lower in the forced experiments, except for March sea ice extent where they tend to be higher. We see the impact of the multicategory ice on the sea ice extent and volume, which are much closer to observations than the single category set up. Comparing the bias in volume and extent the single category version of LIM3 tends to produce ice that is too thin. In the coupled mode, the multicategory model is closer to the observations, but this may be due to compensation of errors. The interannual variability in September sea ice extent is reduced in all models when they are coupled to the atmosphere.

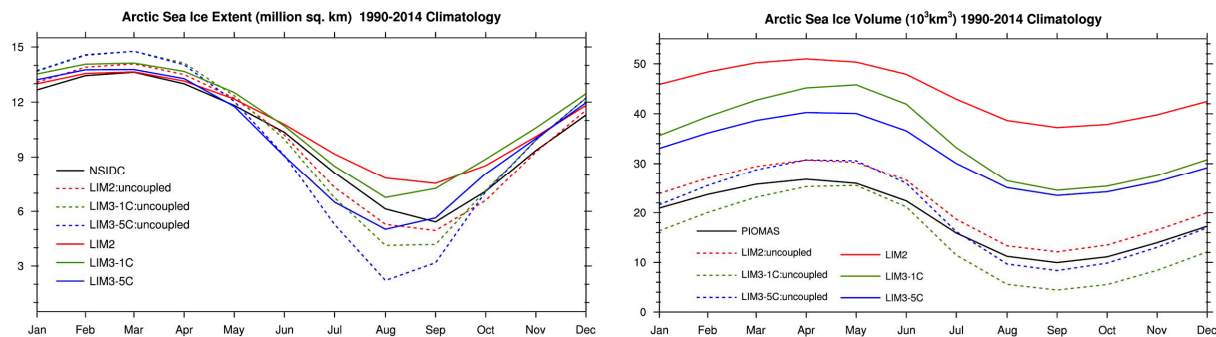


**Figure 8.** Seasonal cycle of SIE and SIV for forced and coupled runs. Observational estimates shown with black solid lines. Forced runs are shown with a dashed line and couple runs with a solid coloured line.

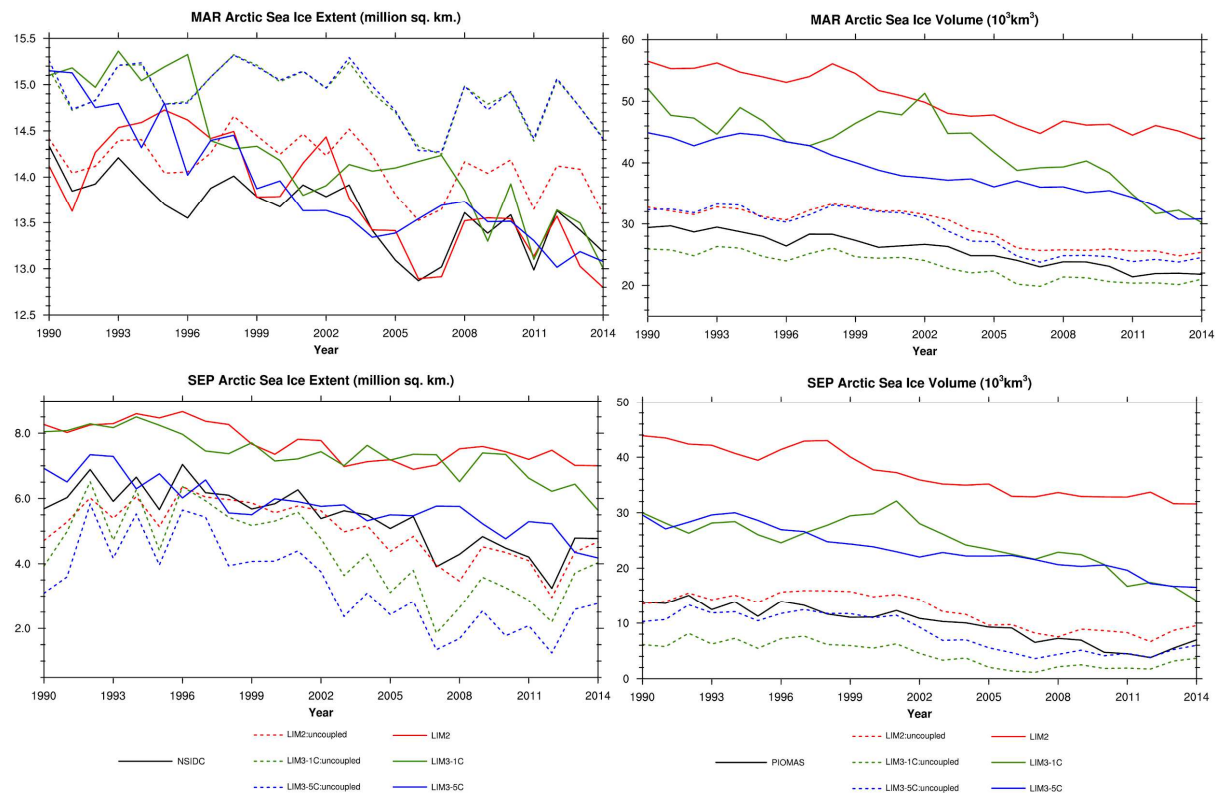


**Figure 9.** Time series for March and September SIE and SIV for 1990-2014 for observational estimate (black line), forced runs (dashed coloured) and coupled runs (solid coloured).

March and September characteristics are shown in Figure 3. It is worth noting that September is the minimum in the cycle, but also includes some refreeze. Biases are lower in the forced run, but we see the impact of the multi-category ice on the sea ice extent and volume which are much closer to observational values than the single category set up. In coupled mode, the multi-category model is much better at capturing the anomalies.

### 3.2.2 Melt pond schemes

The melt pond schemes have been introduced in two different climate models, i.e. LIM3 and CICE4. In the first case, UCLouvain developed and implemented the new schemes in the code and here presents the impact in forced ocean-sea ice simulations, while SMHI analyzed the impact of the schemes in coupled runs. CMCC updated its version of the CICE code used in the climate system (Cherchi et al., 2018) introducing and testing the effect of two melt-pond schemes.

At **UCLouvain**, model experiments have been carried out with NEMO3.6 forced by atmospheric reanalysis and EC-Earth (NEMO3.6 coupled to IFS) with atmospheric forcing fixed at 2000-year values, both using the three melt-pond parameterizations mentioned above and with an ocean resolution of 1° (T255 atmosphere grid for EC-Earth).

The simulations with NEMO3.6 have been run over 1958-2015 with the DFS5.2 reanalysis. The simulations with EC-Earth have been run 27 years at UCLouvain, but the current run duration is not long enough to make robust statements related to the melt-pond parameterizations in EC-Earth. An extension (in time) of these model simulations is ongoing. In the meantime, SMHI has performed a series of model simulations with EC-Earth and the same melt-pond parameterizations (see their contribution in this deliverable), and we actively collaborate with them in the analysis of results.

In the following, our contribution focuses on the NEMO3.6 simulations forced by DFS5.2 reanalysis. We only show results from the empirical and topographic melt-pond parameterizations, as the prescribed parameterization has no relation between the albedo and the surface meltwater fluxes. We compare these simulations to a control run where no melt-pond parameterization is used.

Results of the model simulations run with NEMO3.6 show that there is a slight reduction in sea-ice area in September when using the empirical and topographic melt-pond parameterizations compared to the control run (Fig. 10 right), while there is no difference in March sea-ice area (Fig. 10 left). The two melt-pond parameterizations have very similar sea-ice areas over the whole time series (Fig. 10). The model generally overestimates the observed sea-ice area in March and is in relatively good agreement with NSIDC observations in September (Fig. 10).

In terms of sea-ice volume, there is a reduction when using both parameterizations compared to the control run, and this reduction is more pronounced with the empirical parameterization (Fig. 11). As for sea-ice area, the model generally overestimates the March sea-ice volume compared to PIOMAS reanalysis and is in good agreement with PIOMAS in September (Fig. 11).

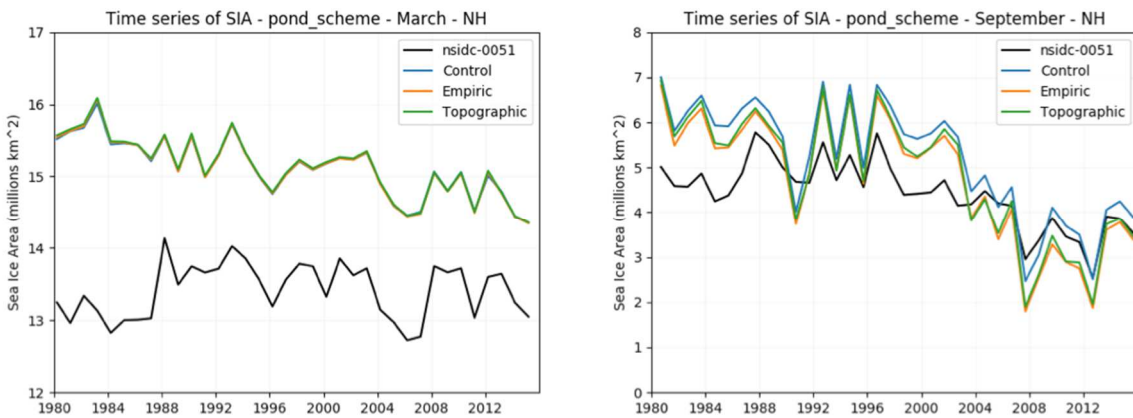


Figure 10. Arctic sea-ice area in March (left) and September (right) for NEMO3.6 (control, empirical and topographic melt-pond parameterizations) and NSIDC-0051 observations.

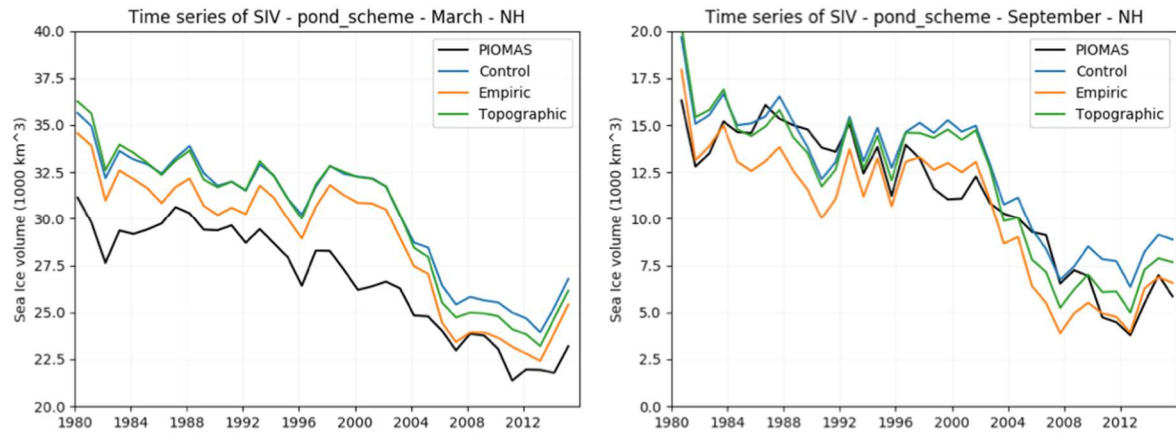
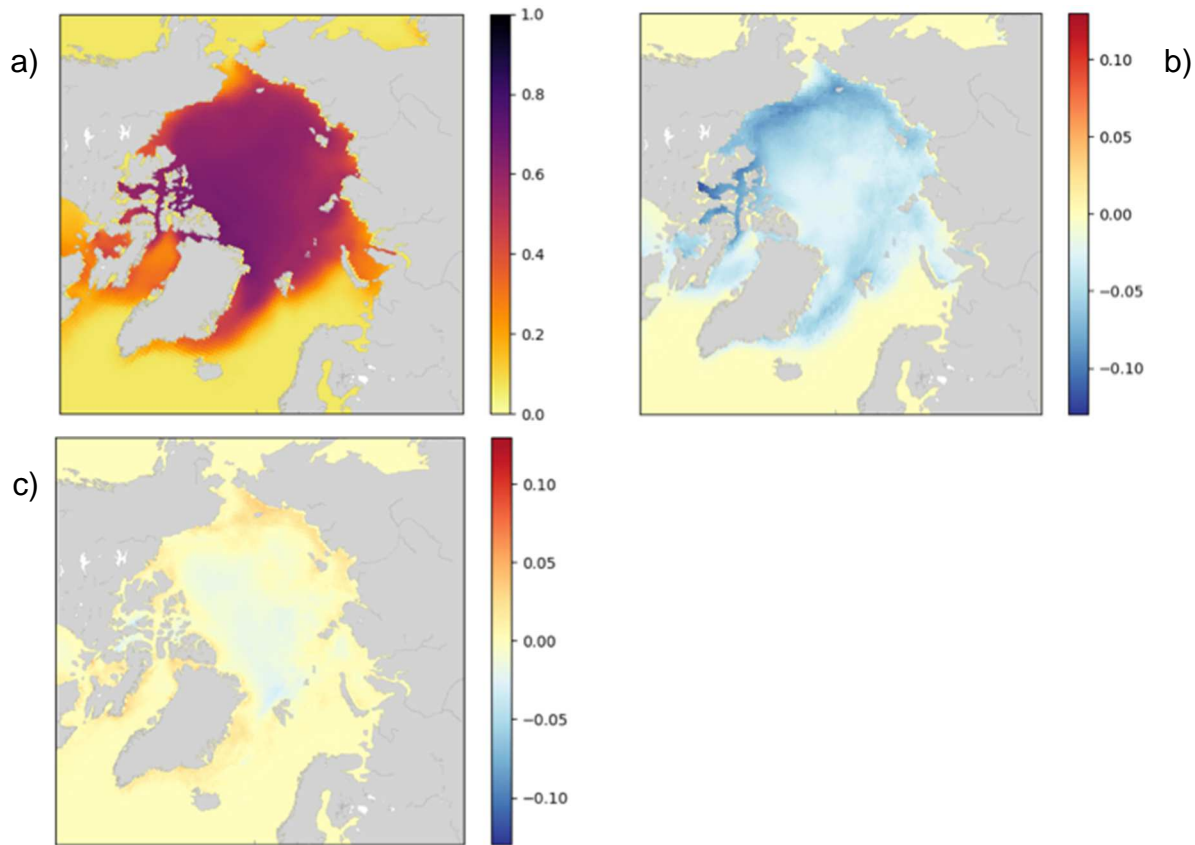


Figure 11. Arctic sea-ice volume in March (left) and September (right) for NEMO3.6 (control, empirical and topographic melt-pond parameterizations) and PIOMAS reanalysis.

Sea-ice albedo (computed as a linear combination of clear-sky and overcast-sky albedos, weighted by the cloud fraction, and based on the parameterization from Shine and Henderson-Sellers, 1985) is reduced by up to 10% with the empirical parameterization compared to the control run, with higher reductions along the sea-ice edge (Fig. 12b). The albedo reduction is much lower with the topographic parameterization compared to the control run (Fig. 12c).



*Figure 12. a) Sea-ice albedo in the Arctic Ocean for the control simulation of NEMO3.6. b) Difference in sea-ice albedo between the simulation with empirical parameterization and the control simulation. c) Difference in sea-ice albedo between the simulation with topographic parameterization and the control simulation (bottom panel). All values are averaged over the summer months (June, July, August) of the period 1985-2015.*

Maps of melt-pond volume reveal that the formation of melt ponds in summer is more pronounced when using the empirical parameterization compared to the topographic parameterization (Fig. 13). This probably partly explains the lower Arctic sea-ice volume with the empirical parameterization compared to the topographic one (Fig. 13).

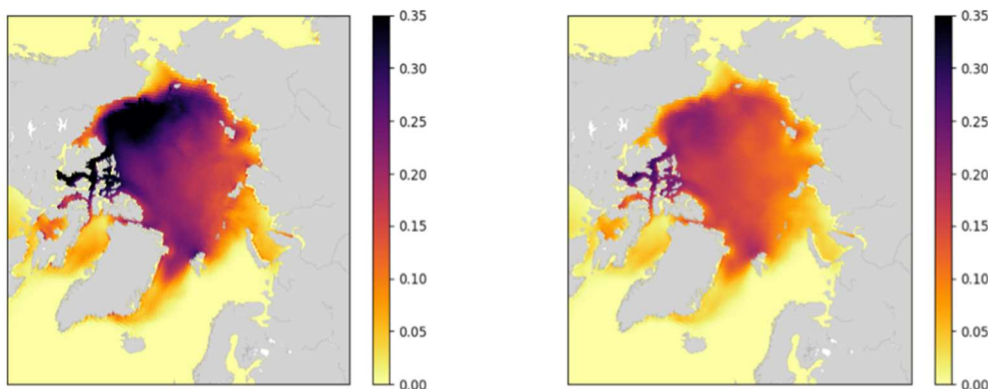


*Figure 13. Melt-pond volume (in m) in the Arctic Ocean for the empirical (left) and topographic (right) melt-pond parameterizations with NEMO3.6, averaged over summer months (June, July, August) of the period 1985-2015.*

The mean melt-pond fraction north of 60N is slightly lower in the topographic parameterization compared to the empirical parameterization. Both parameterizations generally overestimate this quantity compared to MODIS observations over the period 2000-2011, especially in July, but the order of magnitude is similar, with about 15-20% melt-pond fraction in July-August (Fig. 14).

In summary, the use of empirical and topographic melt-pond parameterizations in NEMO3.6 results in lower Arctic sea-ice area and volume compared to a control run without melt-pond parameterization. It also provides a more physical representation of sea ice in summer, with a mean melt-pond fraction that is realistic compared to observations. Further work is needed to understand the impact of these melt-pond parameterizations on sea ice and climate. The plan in the short term is to run NEMO3.6 with two other atmospheric reanalyses (JRA-55 and NCEP/NCAR) in order to test the impact of the atmospheric forcing on model results with the different melt-pond parameterizations. We will also extend our EC-Earth model simulations and compare our results to the ones from SMHI.

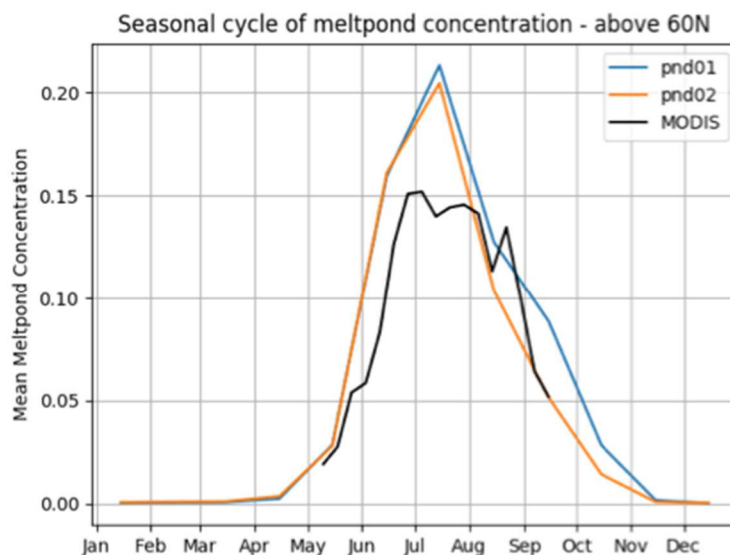


Figure 14. Mean melt-pond fraction north of 60N for the NEMO3.6 simulations with empirical parameterization (pnd01, blue curve) and topographic parameterization (pnd02, orange curve) as well as MODIS observations, averaged over the period 2000-2011.

**SHMI** compared the effects of melt-ponds and increased resolution in EC-Earth.

Here, we used the coupled EC-Earth3-model and performed experiments with and without melt-pond parameterization in both standard and high resolution.

We analyse the role of melt-ponds in controlling the sea ice mass and potential remote effects of melt-pond related sea ice changes, and compare these impacts to the impact of increased resolution on both Arctic and remote climate.

We performed four simulations with the coupled EC-Earth3P model for the transient period 1950-2014 following the HighResMIP-protocol:

- CTRL\_STD: 1950-2014 simulation with the standard-resolution EC-Earth3P (T255 in atmosphere, ORCA 1 in ocean) without melt ponds.
- CTRL\_HR: 1950-2014 simulation with the high-resolution EC-Earth3P (T511 in atmosphere, ORCA025 in ocean) without melt ponds.
- MELT\_STD (MP3\_std): EC-Earth3P standard resolution including melt-ponds (using the topographic parameterization described above)
- MELT\_HR (MP3\_high): EC-Earth3P high resolution including melt-ponds (topographic parameterization)

Note that the CTRL-simulations here are not the control-1950 simulations as defined in the HighResMIP-protocol.

Based on the standard and high resolution simulations, firstly we analysed the impact of melt-ponds on the Arctic Sea Ice Cover (SIC) and Sea Ice Volume (SIV). Compared to corresponding standard resolution runs (CTRL\_STD and MELT\_STD), both high resolution simulations (CTRL\_HR and MELT\_HR) show a year-around reduction in the SIC and SIV (Figure 15). All simulations are characterized by similar marked natural variability at interannual and decadal timescales. We see opposite responses over certain periods between standard and high resolution simulations, which is likely due to natural variability.

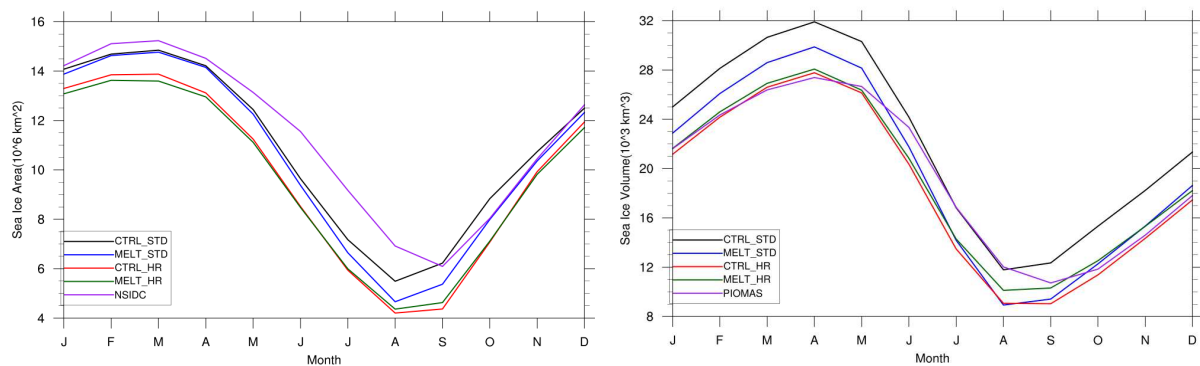


*Figure 15: Arctic Sea Ice extent (left) and volume (right) seasonal cycle in the standard and high-resolution simulations with and without melt-ponds in EC-Earth and observation.*

However, the melt-pond parameterizations exhibit different behaviour in standard and high resolution simulations. This can be seen from Figures 16 and 17, which illustrates the temporal evolution of SIC and SIV in March and September; all simulations are characterized by similar marked natural variability at interannual and decadal timescales. The magnitude of the response to melt ponds is smaller in high resolution. Moreover, melt ponds lead to opposite responses over certain periods between standard and high resolution simulations, which is likely mainly due to natural variability.

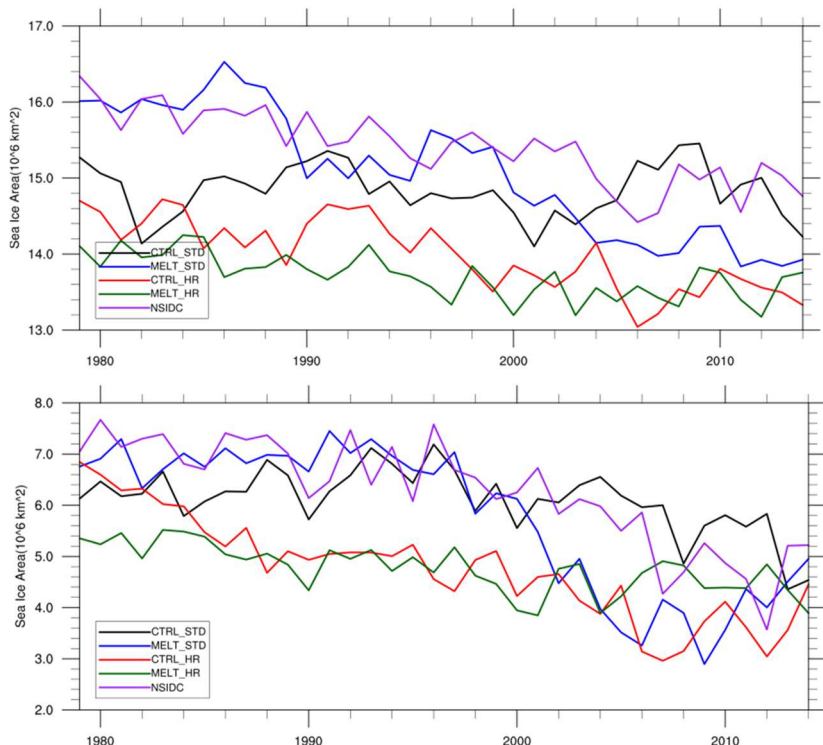


Figure 16. Arctic Sea Ice extent in March (top) and September (bottom) during 1979-2014 in the standard and high-resolution simulations with and without melt-ponds in EC-Earth .

In the high resolution simulation, the melt pond fraction and depth are substantially smaller than in the standard simulations (Figure 18). More detailed spatial distribution of melt ponds fraction (Figure 19) reveals that melt-pond fraction is systematically larger in standard simulation from June to August. Since implementing melt ponds can significantly reduce the surface albedo, this will further impact the formation of melt ponds. However, our simulations clearly show that standard and high resolutions lead to a reversed sea ice albedo response (Figure 20). In standard simulation, sea ice albedo is reduced over large parts of the Central Arctic during the whole summer with melt-pond implementation, while in high resolution simulation the implementation of melt-ponds tends to lead to larger sea ice albedo in the Arctic. This causes less melt-ponds fraction in high resolution simulation. The impact of the melt-pond scheme is still ambiguous and the large internal variability of the Arctic climate system may also play an important role.

The implementation of melt-ponds into EC-Earth leads to a slight reduction of sea ice area and volume in the Arctic compared to a control run without melt ponds. This effect is more pronounced in low resolution than in high resolution.

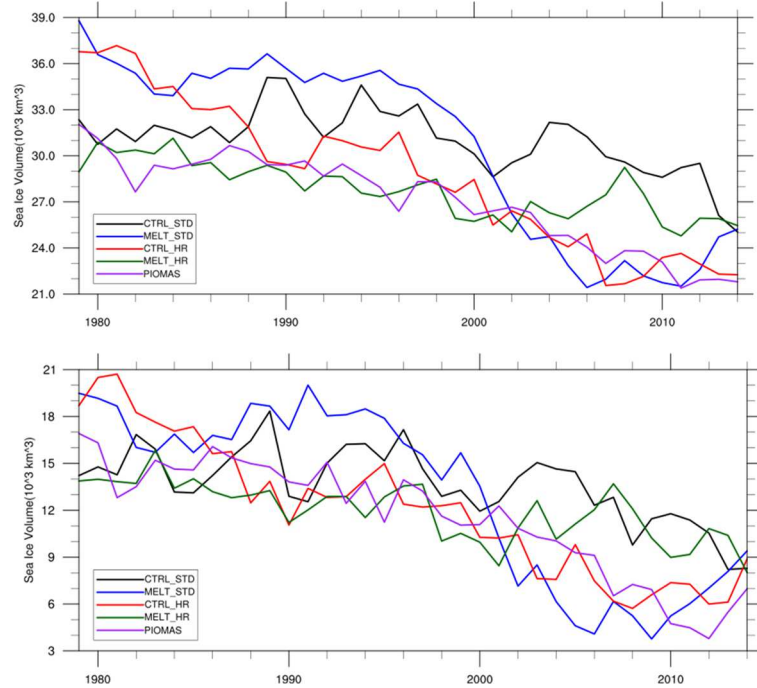


Figure 17: Arctic Sea Ice Volume in March (top) and September (bottom) during 1979-2014 in the standard and high-resolution simulations with and without melt-ponds in EC-Earth.

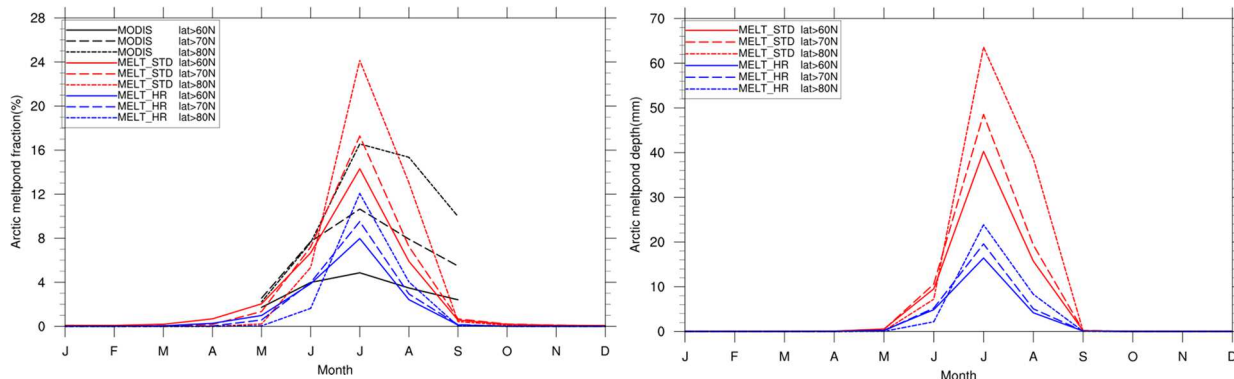
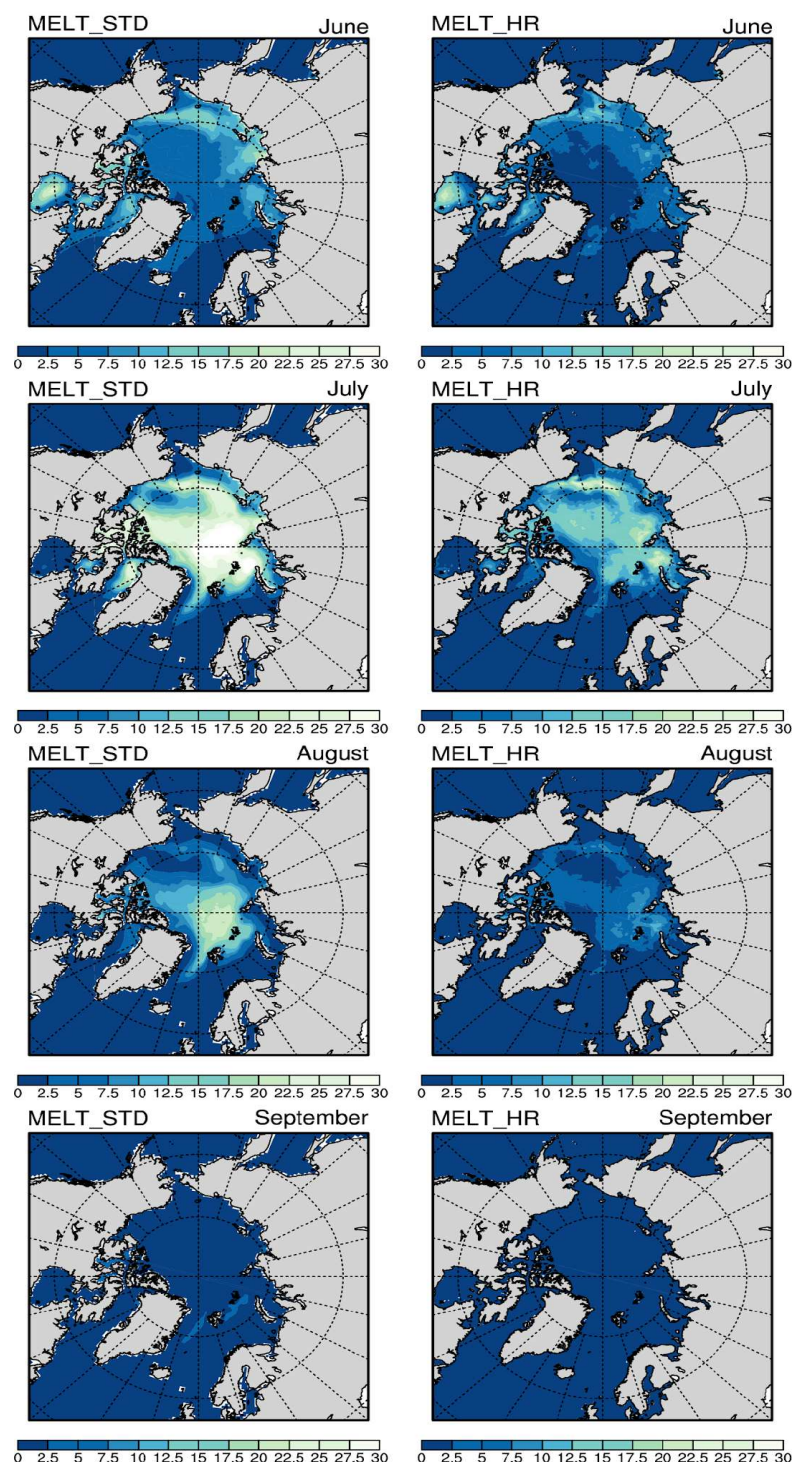
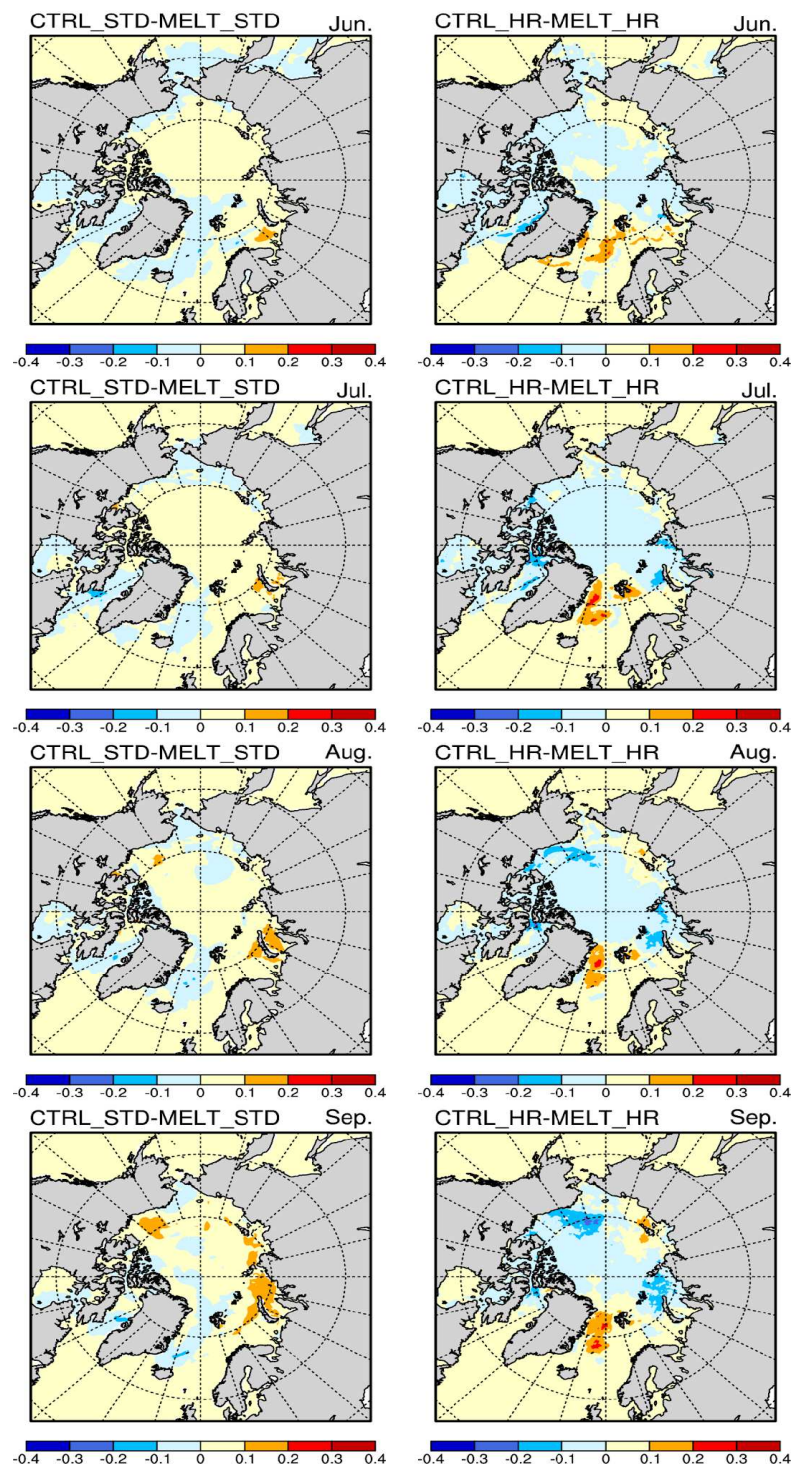


Figure 18: Arctic melt pond Fraction seasonal cycle in the standard and high-resolution simulations, averaged over the period 1991-2010.



*Figure 19. Melt pond Fraction from June to September in standard (left) and high-resolution (right) simulations (unit:%), for the period 1991-2010.*



*Figure 20. Arctic sea ice albedo differences between control runs and melt-pond simulation from June to September in standard (left) and high (right) resolution simulations, averaged over the period 1991-2010.*

**CMCC** carried out a set of experiments, in forced and coupled mode, using the CMCC-CM2 climate model that includes a modified version of CICE4.1 coupled to NEMOv3.6 (at standard 1 degree and high 1/4 of degree resolution, with 50 vertical levels) and CAM5 (at 1 degree). The stability of the two schemes, CESM and TOPO, has been first tested in stand-alone mode with imposed atmospheric and oceanic forcing. Then, we performed twin simulations (with the 2 schemes) of the ocean-sea ice system (NEMO-CICE) driven by CORE-II atmospheric forcing at standard resolution, over the period 1975 – 2009. Then, we performed climate runs over the period 1980 – 2005, for both the standard-resolution and the high-resolution configurations. The EVP rheology and 5 ice thickness categories are used in all runs.

TOPO, the physically based melt pond scheme, which simulates the evolution of melt ponds based on sea ice conditions, significantly impacts the Arctic sea ice characteristics and their variability. In both model configurations, at low (not shown) and high resolutions, the topographic scheme results in a reduction of sea ice during the all period of integration. Time series of March and September sea ice area show that TOPO scheme generally results in reduced sea ice area, especially in September, at the end of the melting season (Fig 21). Sea ice concentration is largely affected in summer, with the strongest reduction located at the ice edge. Consequently, ice thickness decreases from the CESM to TOPO everywhere in the Arctic basin (up to 1m), as the summer spatial distribution shows in Figure 22. It is with noting that, in this configuration, our model overestimates sea ice area and volume (not shown) with both melt pond schemes, in comparison to satellite data and results from PIOMAS reanalysis. To assess the impact on processes driving melt and how this varies spatially and temporally, the thermodynamic response is decomposed in surface, bottom and lateral components of the total melt. The bottom melt is the strongest contributor to the total melt - reaching up to ~1.2 cm /day in JAS in TOPO, while the contribution from lateral melt is the smallest - up to ~0.4 cm/day in JAS in TOPO. The differences in basal melt and snow/ice temperature at the surface are presented in Fig. 22c,d. The interannual variability of the summer sea ice characteristics (area, extent and volume) is dominated by the surface melt processes.

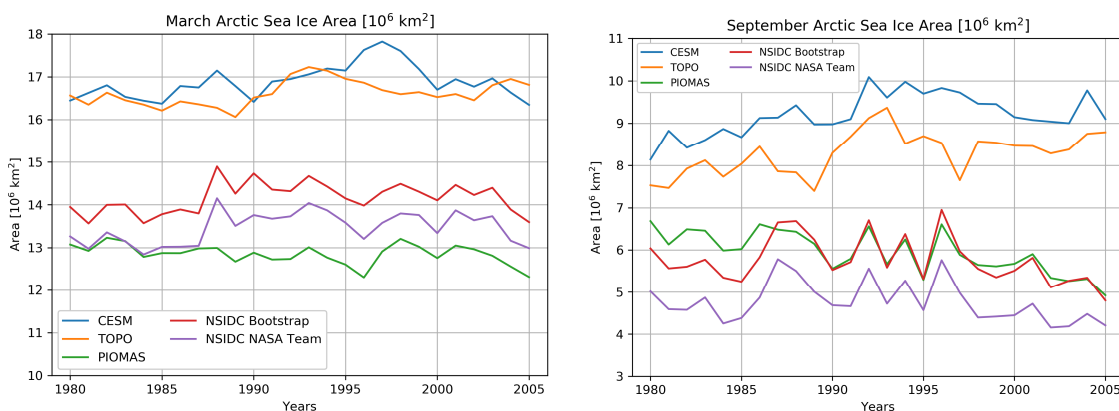


*Figure 21. Time series of Arctic sea-ice area in March (left) and September (right) for the high-res coupled CMCC model with the CESM and TOPO melt-pond parameterizations. NSIDC data and PIOMAS output are also shown.*

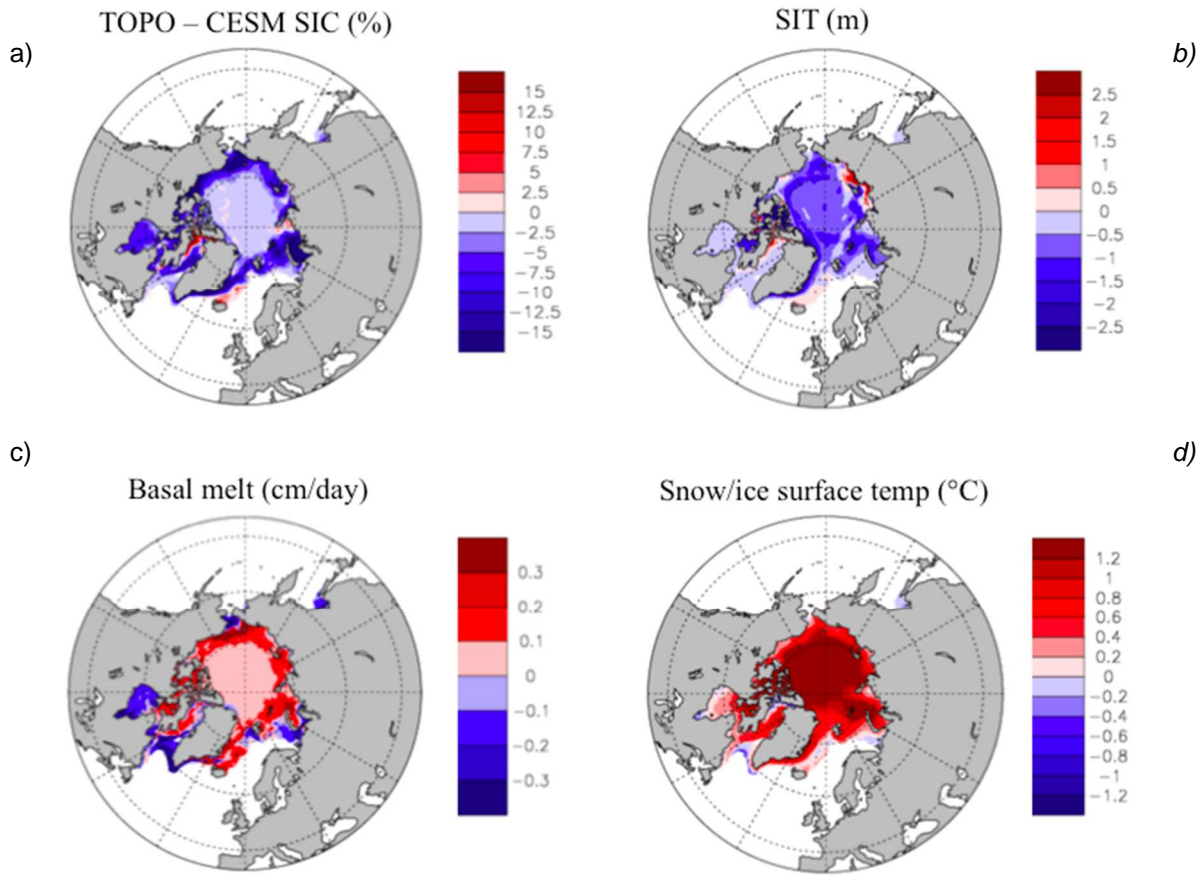


*Figure 22. Differences of summer sea ice properties: a) sea ice concentration (in %), b) sea ice thickness (in m), c) basal melt (cm/day), and d) snow/ice surface temperature, between TOPO and CESM coupled experiments at high resolution, averaged over the period 1980–2005.*

With both schemes, melt pond fraction start to increase in the May/June, reach a maximum extent in July and refreeze during August as shown in Figure 23, in agreement to UCLouvain runs based on LIM3 and MODIS observations. CESM parameterization produces a slightly smaller melt pond concentration in winter and fall, and is about 10% larger in July. Comparing the spatial distribution of the July melt pond fraction, CESM generally presents a larger fraction of melt pond in the Arctic basin. The fraction reduction in TOPO is evident in the Beaufort Gyre and in the Nordic Seas, and in the Barents Sea where TOPO present a larger pond concentration (Fig. 24).

Based on the CMCC climate model results, the benefits of the TOPO melt pond formulation are evident in reproducing the Arctic ice mean state and variability, with a reduction of sea ice extent and volume that are generally overestimated in our climate simulations. Our version of the topographic scheme is ready to be used (in conjunction with the Delta-Eddington multiple scattering radiative transfer model), but it is worth mentioning that impact of both melt pond schemes on the Antarctic sea ice requires more analysis.

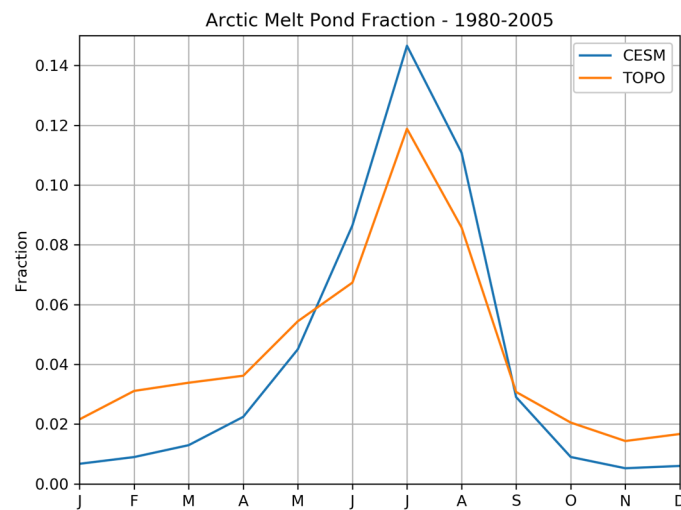


Figure 23 Seasonal cycle of Arctic melt-pond fraction for the CESM and TOPO simulations with the CMCC-CM model, averaged over the period 1980-2005.

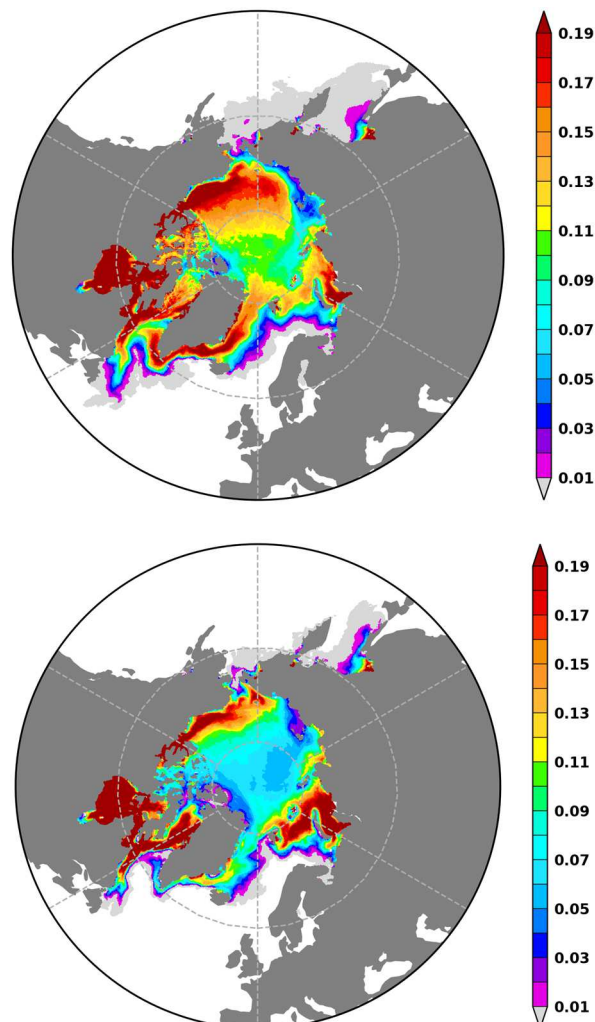


Figure 24. Arctic melt-pond for the CESM (top) and TOPO (bottom) melt-pond parameterizations in the coupled high-res CMCC runs, averaged in July over the period 1985-2015.

### 3.2.3 Rheology

**MetOffice** implemented an Elastic-Anisotropic-Plastic (EAP) rheology.

The representation of sea ice dynamics in most modern climate models use the viscous-plastic (VP) style of rheology (Hibler, 1979) – based upon the early continuum model approach of the AIDJEX model (Coon et al., 1974). The basic assumption made within these isotropic models is that model grid-cells are large enough to contain a representative sample of ice types, with a sufficiently large number of leads and ridges for there to be no preferred orientation. In such a situation, it is acceptable to use the isotropic theory that forms the basis of the commonly used VP family of rheologies – such as the Elastic-Viscous-Plastic (EVP) rheology used within the CICE model, the sea ice component of the HadGEM3 climate model. However, for models being run at sufficiently fine resolution, grid cells can no longer contain a representative sample of ice types and orientations. The question then arises as to whether an isotropic sea ice rheology, designed for coarse resolution, should be used with high-resolution climate models. The Elastic-Anisotropic-Plastic (EAP) rheology was developed to explicitly account for the sub-grid scale anisotropy of the sea ice cover (Wilchinsky and Feltham, 2006; Tsamados et al., 2013), making it more appropriate than EVP for high-resolution climate simulations. Motivated by satellite imagery, the sea ice cover in the EAP rheology is assumed to comprise of diamond-shaped ice blocks formed from intersecting slip lines. The orientational distribution of these diamond-shaped floes, and hence the degree of anisotropy, is described using a structure tensor that evolves over time. This approach allows the EAP rheology to explicitly account for the sub-continuum anisotropy of the sea ice cover whilst avoiding detailed modelling of fracture processes.

The EAP rheology has been included within the GC3.1 configuration of the HadGEM3 physical climate model, which is the version used as the UK's physical climate model contribution to CMIP6. Several technical upgrades to the EAP formulation, provided by the Centre for Polar Observation and Modelling (CPOM) – the original developers of the EAP rheology, have also been incorporated into HadGEM3 to improve the computational efficiency of the EAP model. Two 50-year equilibrium climate runs, with constant greenhouse gas forcing representative of the year 2000, have been performed using the EAP rheology. This has been done using both the low-resolution (N96-ORCA1) and the medium-resolution (N216-ORCA025) HadGEM3 configurations that are being used for CMIP6 runs. The sea ice simulation in the EAP experiments are compared to existing HadGEM3 runs performed with the standard EVP rheology.

Comparison of the sea ice simulations in the EAP and EVP rheology experiments suggest that the EAP rheology is improving the distribution of sea ice thickness in the Arctic by better representing the thicker ice north of Greenland and the Canadian Arctic archipelago, and increasing the gradient of ice thickness across the Arctic Ocean basin (Figure 25). This improvement of the thicker ice north of Greenland is associated with a reduction in the speed of the sea ice within the central Arctic Ocean in the EAP simulations (Figure 26).

Sea ice extent and volume are shown in Figures 27 and 28 respectively. Several EVP control runs are included for each resolution to help put the rheology-induced differences into context with respect to the internal variability of Arctic sea ice cover. Given the large influence of internal variability on Arctic sea ice, there is no discernible change in either of these basin-wide integrated quantities (i.e., extent or volume) when using EAP rather than EVP for the low-resolution ORCA1 system. Although, after 15 years into the ORCA1 simulation, the volume is quite different for the EAP model compared with either of the EVP runs, the EAP

volume sits almost exactly between that for the two EVP runs (Figure 28). Interestingly the EAP rheology behaves differently for the higher resolution ORCA025 model runs, which show an overall increase in volume not seen in the low-resolution ORCA1 runs (Figure 28). Figure 28 shows a rapid increase in volume – for all times of the year – over the latter part of the first decade of the simulation. This increase in basin-scale volume is also apparent as a general thickening of the sea ice throughout the Arctic basin (Figure 25). This thickening seems to be associated with an increase in the proportion of thicker, deformed ice caused by an increase in the ridging rate (Figure 29).

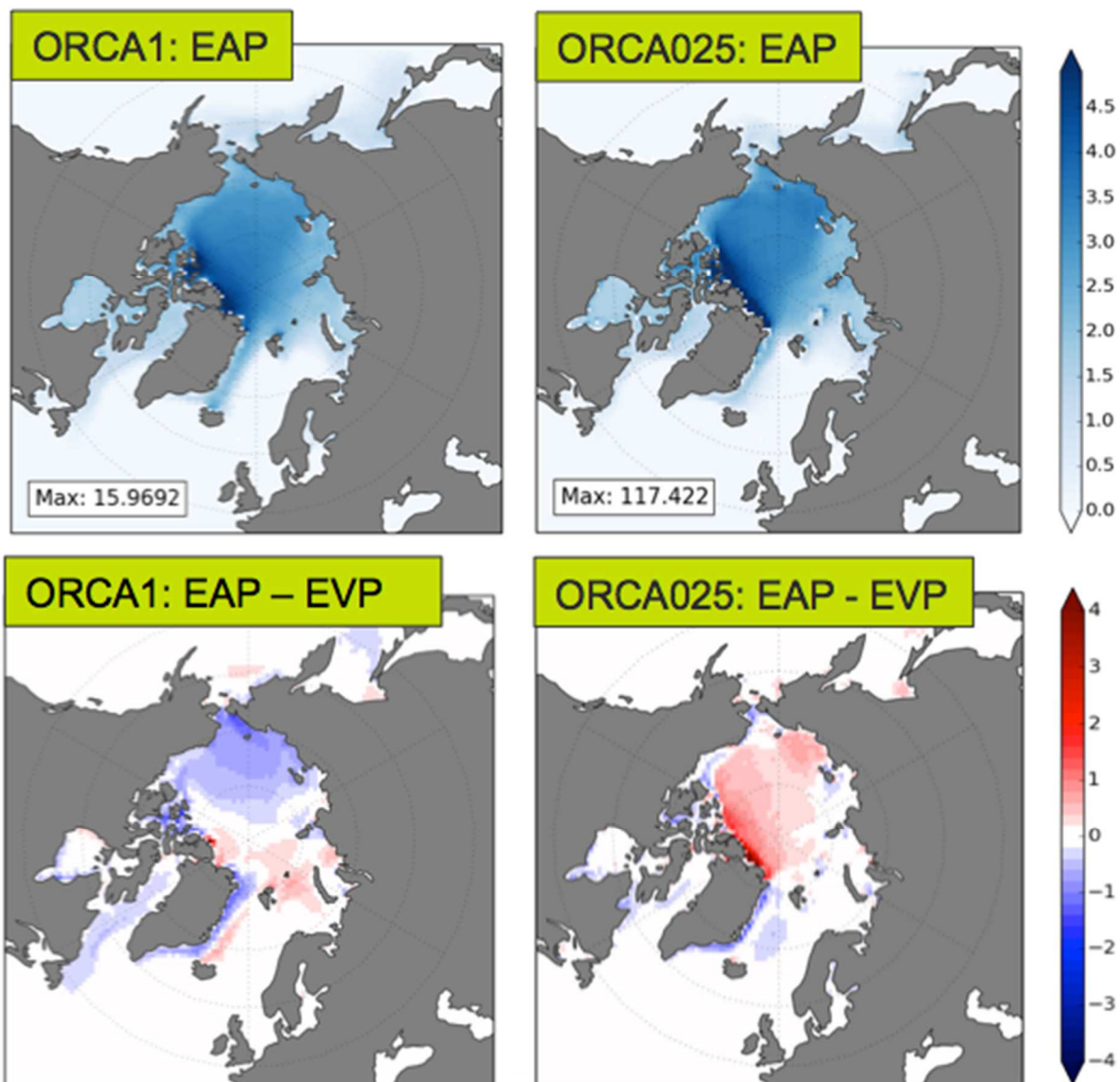


*Figure 25. March Arctic sea ice thickness (m) with EAP rheology (upper plots) in the HadGEM3 physical climate model with 1 degree (ORCA1, left) and 1/4 degree (ORCA025, right) resolution. Differences between the EAP and EVP rheology simulations are also shown (lower plots). Differences are calculated as EAP-EVP so areas of red (blue) denote that the sea ice in the EAP simulation is thicker (thinner). Results are shown from years 16-30 of each integration after the model had spun-up for 15 years.*

Evaluation of the results using the EAP rheology in HadGEM3 suggest that it could be beneficial to include the EAP rheology within climate models, as it improves the spatial distribution of ice thickness in the Arctic basin. Although promising for thickness distribution there are a number of points that need further investigation. Firstly, the ice speed in the central Arctic Ocean basin has been greatly reduced (Figure 26). The fact that ice speed has reduced is consistent with the findings of Tsamados et al. (2013) – who, in a stand-alone sea ice model, showed that using EAP gave a reduction in ice speed of up to 50% in some regions, bringing the model into closer agreement with satellite observations (see Figure 30c). However the reduction in speed that we see in the HadGEM3 coupled climate model experiments is much more extreme than was reported by Tsamados et al. (2013), meaning that ice speed is no longer in good agreement with observations (Figure 30).

Secondly, the fact that the impact of switching rheology from EVP to EAP is very different for the higher-resolution ORCA025 model than for the low-resolution ORCA1 model, needs further investigation. At the very least, the ORCA025 model would need to be tuned to provide a realistic model climatology of sea ice thickness. This could either be done by tuning existing parameters such as snow albedo, or to tune the ice thickness within the EAP rheology by varying the parameter  $C_f$  that sets the ridging strength of the ice (following Tsamados et al., 2013).

Finally, it should be noted that, thus far, only the Arctic sea ice has been analysed in the EAP rheology experiments. The potential impact on the Antarctic sea ice has not been investigated within the PRIMAVERA project.

Results are shown from years 16-30 of each integration after the model had spun-up for 15 years.

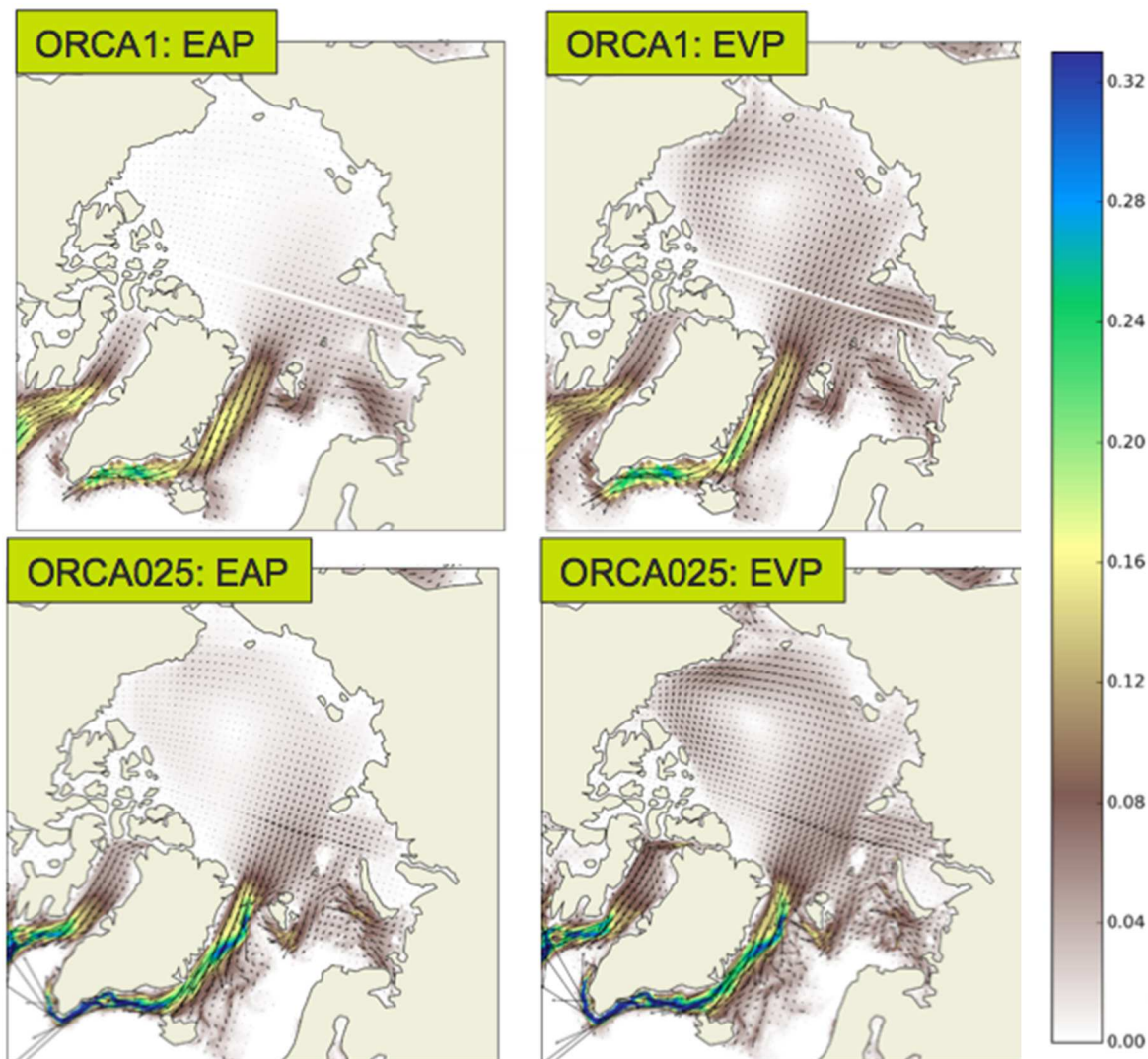
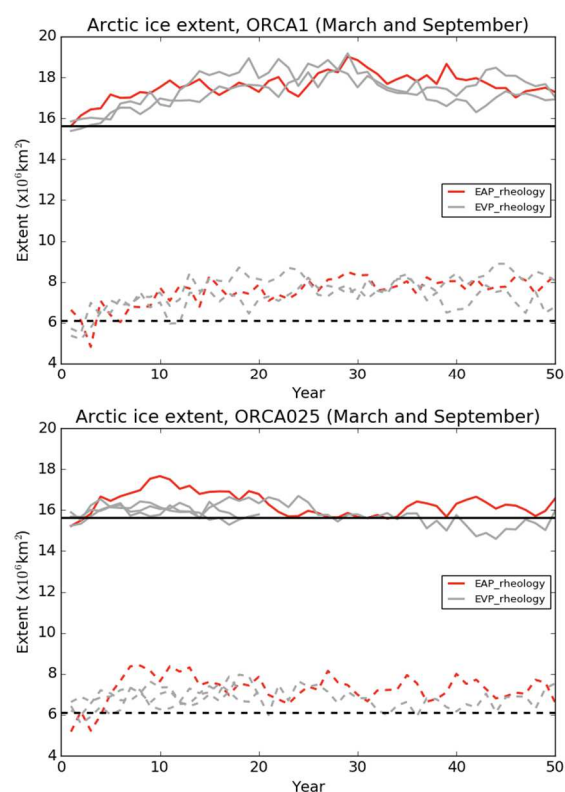
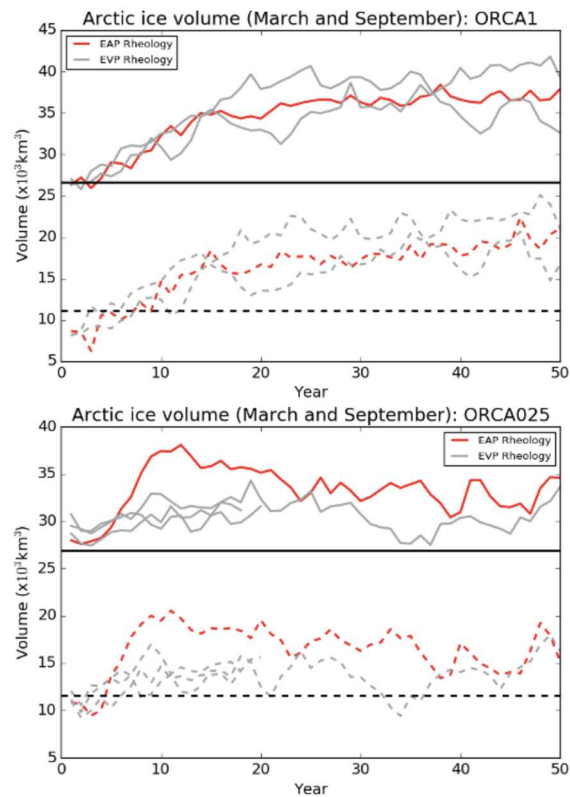


Figure 26. Arctic ice velocity (arrows) and speed (shading; m/s) in HadGEM3 for ORCA1 (top) and ORCA025 (bottom) resolutions, and for the EAP (left) and EVP (right) rheologies. At both resolutions, using the EAP rheology has reduced the ice speed in the Arctic Basin.



*Figure 27. Time series of Arctic sea ice extent for March (solid lines) and September (dash lines) for HadGEM3 at two resolutions: ORCA1 (top), and ORCA025 (bottom). Results from the EAP experiment are in red, and results from a number of parallel EVP experiments are in grey. The horizontal black lines represent observed sea ice extent from the HadISST1.2 dataset (Rayner et al., 2003) for the period 1990-2009.*



*Figure 28. Time series of Arctic ice volume for March (solid lines) and September (dash lines) for HadGEM3 at two resolutions: ORCA1 (top), and ORCA025 (bottom). In each case, results from the EAP experiment are shown in red, and results from a number of parallel EVP experiments are shown in grey. Mean ice volume for 1990-2009 from the PIOMAS, as a reference, is shown by the horizontal black lines.*

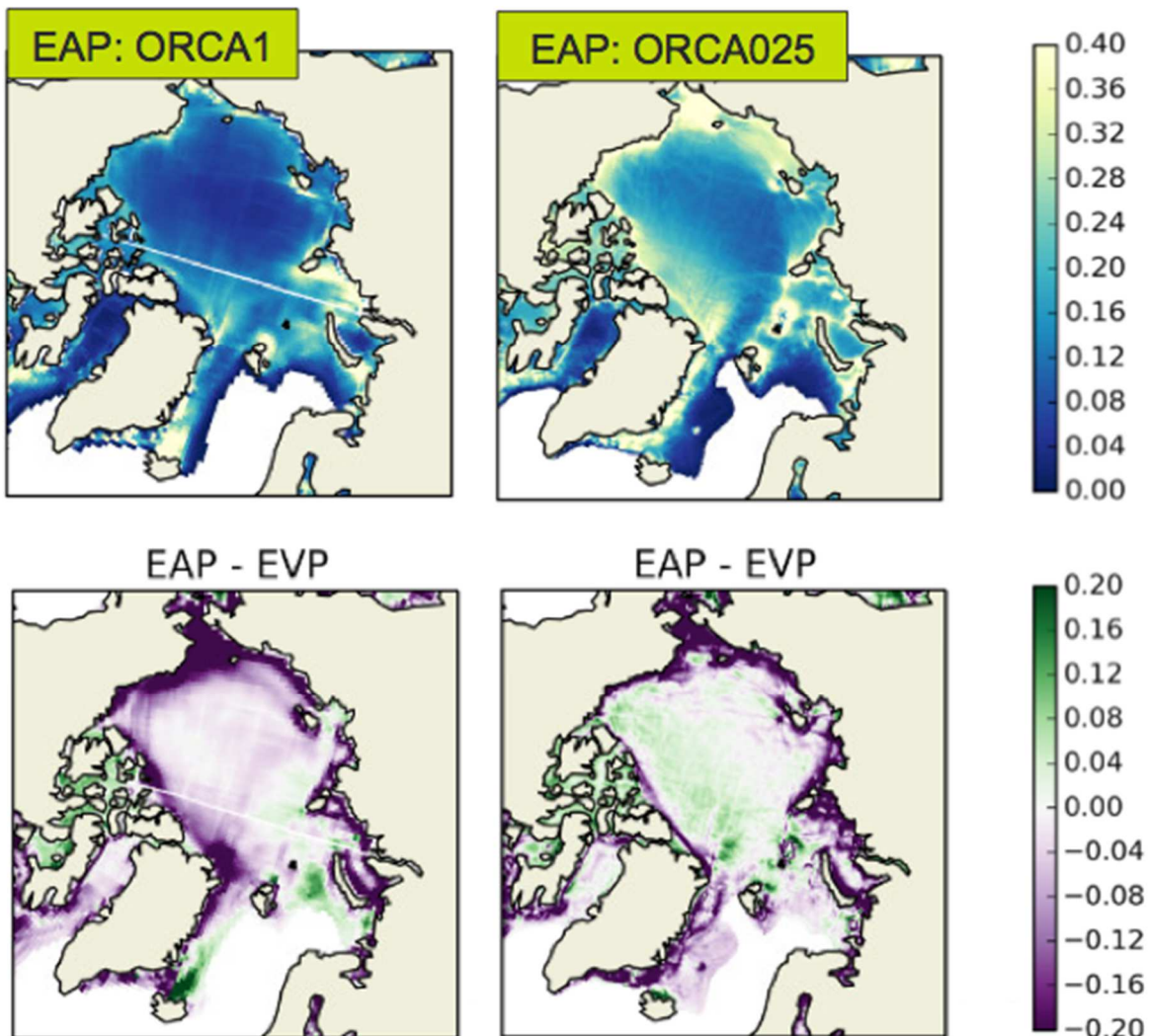
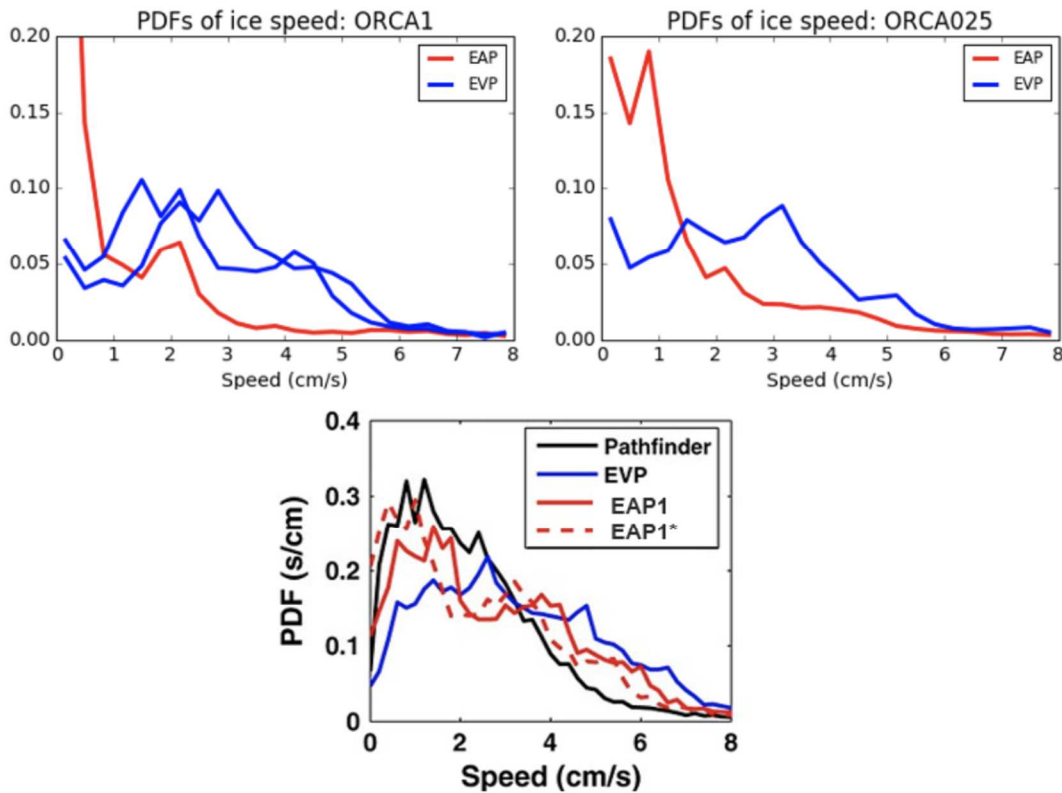


Figure 29. Ice volume ridging rate (cm/day) in March for ORCA1 (left), and ORCA025 (right) resolutions. Showing the results using the EAP rheology (top) and differences between EAP and EVP (bottom). Differences are calculated as EAP-EVP, meaning that areas of green (purple) denote that there is more (less) ridging when using the EAP rheology. Results are shown from years 16-30 of each integration after the model had spun-up for 15 years.



*Figure 30. (Upper) Probability distribution functions (PDFs) of March sea ice drift speed north of 70°N with the EAP (red lines) and EVP (blue lines) rheologies separately for the ORCA1 (left) and ORCA025 (right) resolution experiments. Also shown (lower) is a reproduction of Figure 8 from Tsamados et al. (2013), showing PDFs of ice speed for their EVP and two different EAP experiments, together with the Pathfinder observational dataset. These data are for April, and for latitudes north of 78°N. (NB. EAP was called “EPA” in Tsamados et al., 2013.)*

At **UCLouvain**, a Maxwell-elasto-brittle (MEB) rheology has been implemented in LIM3. As already highlighted in the PRIMAVERA technical report and Milestone MS7, results with NEMO have revealed physical and technical issues that do not allow to continue within this direction for the rest of the PRIMAVERA project. Using physical parameters to calibrate the MEB leads to the development of instabilities and crashes of the simulations. In order to stabilize the model, non-physical parameter values are needed, at the expense of unrealistic results.

As shown in Figure 32, the total rate of deformation in the Canadian basin with the MEB rheology exhibits unrealistic cross-shaped patterns around the concentrators of deformation. Consequently, this critical behavior and the impossibility to adjust the parameters to realistic values make the MEB implementation with NEMO (and EC-Earth) unsuitable for climate simulations in the current state.

The comparison of MEB with EVP (in NEMO) does not show a dramatic enhancement of the results, while the computing time necessary to run the MEB rheology is quite substantial compared to EVP rheology.

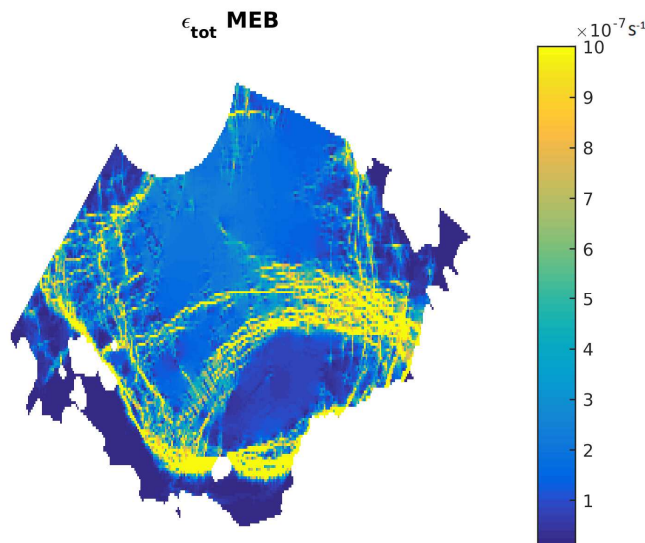


*Figure 32. Simulated total rate of deformation in the Canadian Basin with the MEB rheology implemented in NEMO for the 13th of January 2007, showing some unrealistic cross-shaped patterns around the concentrators of deformation.*

### 3.3 Results: Impact on the atmosphere

ECMWF investigated the impact of ITC on atmospheric fields.

Results show that there is a general improvement in 2mT over the Arctic when we move to the multicategory ice model in the coupled model runs. There is a seasonal dependence on model bias and LIM3 tends to reduce the cold bias in winter and spring that was seen in LIM2 (not shown). The differences between the LIM3 single category and multicategory climates over the Arctic are more pronounced over winter and autumn. The autumn changes relative to LIM2 are that the LIM3 single category increases the cold bias over the Arctic but the multicategory model improves it, this can be explained with better representation of volume which will control the local fluxes of heat.

In the summer months the surface temperatures are less governed by the ocean atmosphere fluxes so potential impacts through the large scale circulation and moisture (cloud feedbacks) may play more of a role. The cold biases in the Barents Sea are slightly reduced in summer using the multicategory model.

Over the southern hemisphere we see a warm bias which is seen when we move from LIM2 to LIM3 for the southern ocean, in Antarctica it is less clear that the multicategory model is better. LIM3 (and LIM3 multicategory setup) is more responsive to the warm bias that exists in the southern ocean and we have very little ice cover in the southern ocean in summer.

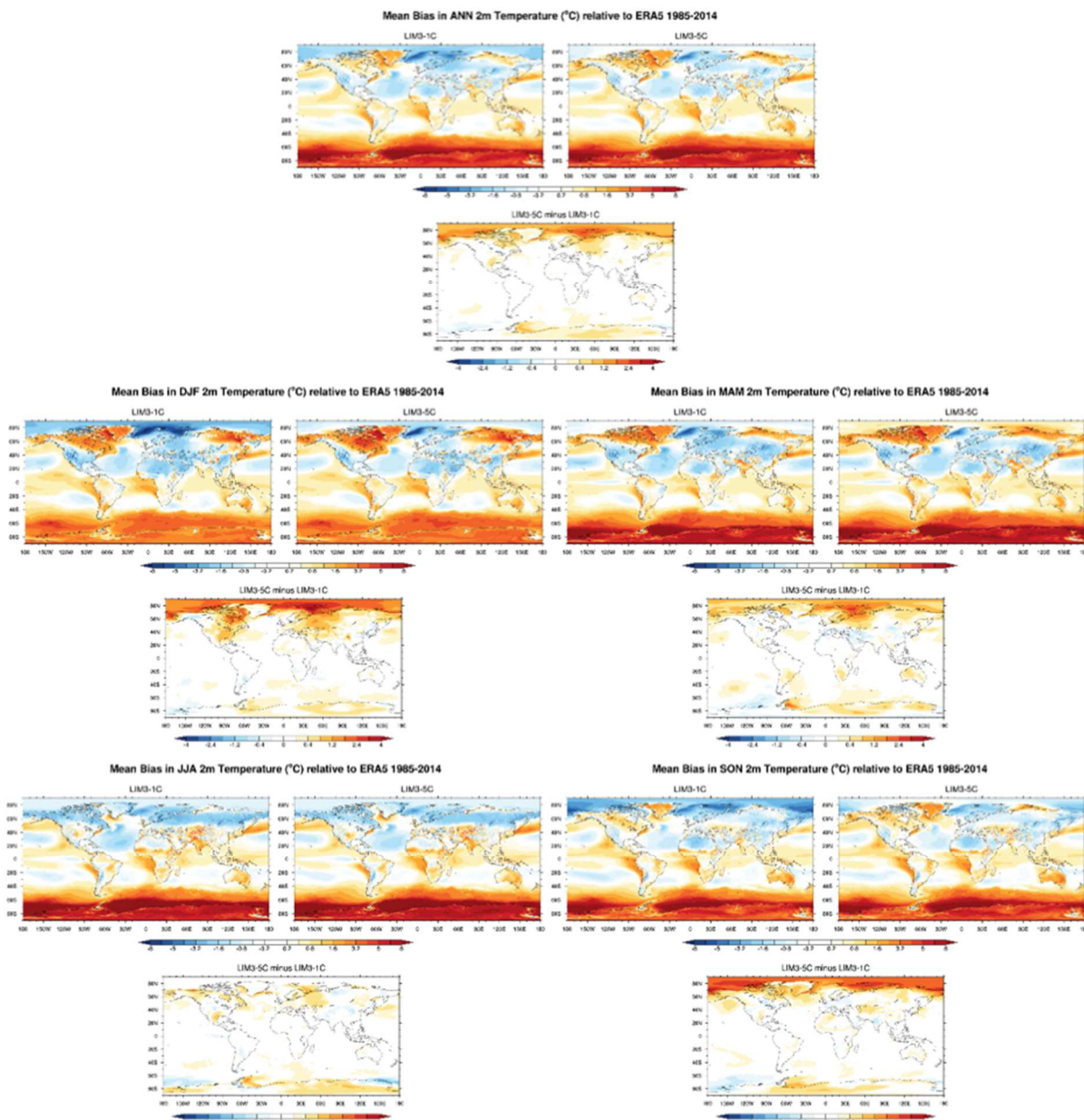


*Figure 33. Difference in 2m Temperature climatology relative to ERA5 for the period 1985-2014 for the Annual and seasonal means. Differences between the model climatologies for single and multi-category LIM3 also shown.*

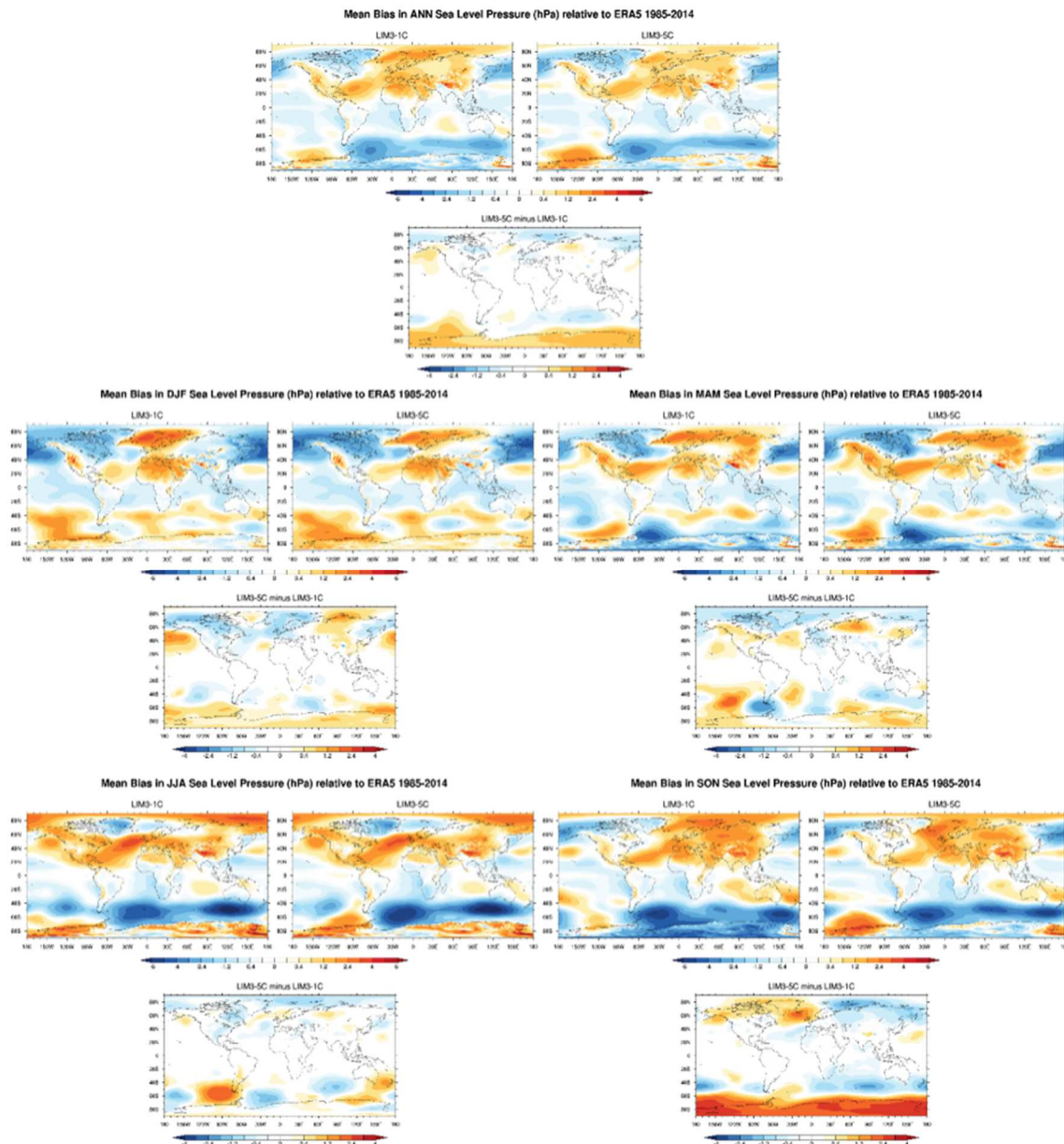


*Figure 34. Difference in MSLP climatology relative to ERA5 for the period 1985-2014 for the Annual and seasonal means. Differences between the model climatologies for single and multi-category LIM3 also shown.*

**SMHI** analysed the impact of melt ponds on temperature.

The sea ice response to increased resolution and melt-ponds leads to a pronounced local temperature effect. Enhanced surface fluxes from the ocean to the atmosphere, when sea ice area is reduced, lead to a warming and vice versa. This effect is particularly pronounced in winter when ocean-atmosphere temperature gradients are largest (Figure 35). In Barents, Greenland and Bering Seas, the winter time temperature response to melt-ponds and to increased resolution is of similar amplitude. In the Barents Sea, both increased resolution and melt-ponds lead to reduced sea ice and increased temperature, which reduces the cold bias in CTRL\_STD in this region. In the Greenland and Bering Seas, the temperature response to

melt-ponds depends on the resolution. While we see a temperature increase (and thus a reduction of the bias) in MELT\_HR in both Greenland and Bering Sea, we see additional cooling in MELT\_STD.

Also, the remote effect of melt-ponds on mid-latitude temperature depends on the resolution. For north-eastern Europe/north-western Siberia, implementation of melt ponds leads to a winter warming and a reduction of the cold bias in this region in standard resolution. In high resolution, we see a warming over south-eastern Europe/ southwestern Asia leading to an increased warm temperature bias.

Increasing resolution leads to a more widespread response with somewhat stronger temperature signals compared to the effect of melt ponds. As for the melt-ponds, it depends on the region, if this signal leads to decreased or increased temperature biases. Along the east coast of the USA and Canada, high resolution causes a cooling, which reduced the warm bias in this region and which is due to a more realistic position of the Gulf Stream in CTRL\_HR (not shown).

Implementation of melt-ponds and related sea ice changes and surface heat fluxes might affect even lower latitudes by affecting the large scale atmospheric and oceanic circulations. However, our results indicate that the remote impact of melt-ponds on lower latitudes is very small. The signal due to increased resolution is substantially larger than the effect of melt-ponds in lower latitudes (not shown).

Generally, the results for the other three seasons agree with winter: in mid and higher latitudes, the effects of melt ponds and increased resolution are of similar amplitude while in lower latitudes, the impact of melt-ponds is small.

The melt-pond implementation seems to lead to some systematically different responses depending on the resolution. In MELT\_HR, a warming in the Nordic Seas and in the Atlantic Arctic Sector occurs in all seasons. In MELT\_STD, we see instead a warming from the Barents Sea eastwards along the Siberian coast and mostly colder temperatures compared to CTRL\_STD in the Canadian Archipelago, Baffin Bay and partly also in the Greenland Sea.

In lower latitudes, temperature and circulation responses to increased resolution are substantially larger than the impact of melt-ponds.

The changes caused by both melt ponds and increased resolution can, depending on the region, increase or decrease biases in the standard model version of EC-Earth. Locally, we found systematic reductions of the biases, e.g.: both melt-ponds and high resolution lead to improved sea ice concentration in the Barents Sea and reduced cold biases in EC-Earth; a better position of the Gulf Stream in the high resolution simulations improves the warm biases along the east coast of North America.

The large natural variability complicates the interpretation of the results and might contribute to the different responses of ice, temperature and circulation to melt ponds and increased resolution. To make more robust statements on the potential effect of melt ponds on the atmospheric circulation and lower latitude climate, ensembles of simulations with and without melt ponds would be necessary.

Further, it is generally difficult to compare a model version that has been tested and tuned to the same version with a physical improvement and expect an improvement in the simulated climate.

The analysis here shows that EC-Earth runs stable with melt ponds implementation and provides reasonable results in both standard and high resolution. Next steps (after

PRIMAVERA) are to include the melt ponds into an upcoming NEMO-release and future EC-Earth (and other coupled model) versions.

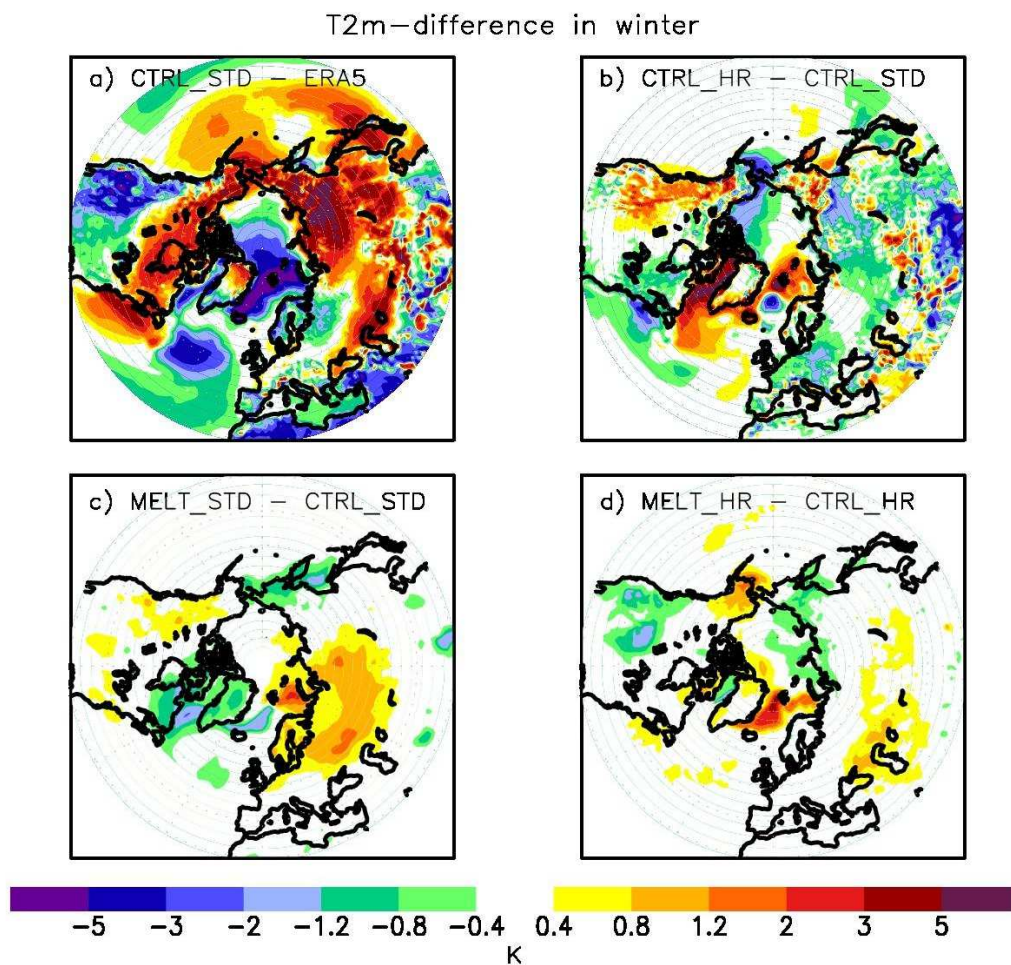


*Figure 35. Winter differences of two meter air temperature (T2m), averaged over 1980-2014:  
a) CTRL\_STD – ERA5, b) CTRL\_HR – CTRL\_STD, c) MELT\_STD – CTRL\_STD, d)  
MELT\_HR – CTRL\_HR.*

## References

- Bader, J., Mesquita, M. D., Hodges, K. I., Keenlyside, N., Østerhus, S., and M. Miles, 2011. A review on Northern Hemisphere sea-ice, storminess and the North Atlantic Oscillation: Observations and projected changes. *Atmospheric Research*, 101(4), 809-834.
- Cavalieri, D. J., C. L. Parkinson, P. Gloersen, and H. J. Zwally, 1996 updated yearly. Sea Ice Concentrations from Nimbus-7 SMMR and DMSP SSM/I-SSMIS Passive Microwave Data, Version 1. Boulder, Colorado USA. NASA National Snow and Ice Data Center Distributed Active Archive Center.
- Cherchi A., T. Lovato, P.G. Fogli, D. Peano, S. Gualdi, S. Masina, E. Scoccimarro, S. Materia, D. Iovino, and A. Navarra, 2018. Global mean climate and main patterns of variability in the CMCC-CM2 coupled model. *Journal of Advances in Modeling Earth Systems*. doi:10.1029/2018MS001369
- Close, S., Houssais, M. N., and C. Herbaut, 2017. The Arctic winter sea ice quadrupole revisited. *Journal of Climate*, 30(9), 3157-3167.
- Coon, M., G. Maykut, and R. Pritchard, 1974. Modeling the pack ice as an elastic-plastic material, AIDJEX Bull.
- Dussin, R., Barnier, B., Brodeau, L., and J.M. Molines, 2016. The Making Of the Drakkar Forcing Set DFS5.2. DRAKKAR/MyOcean Report.
- EUMETSAT Ocean and Sea Ice Satellite Application Facility. Global sea ice concentration reprocessing dataset 1978-2015 (v1.2, 2015). Norwegian and Danish Meteorological Institutes.
- Fichefet, T., and M.A. Morales Maqueda, 1997 : Sensitivity of a global sea ice model to the treatment of ice thermodynamics and dynamics. *Journal of Geophysical Research*, 102, 12,609-12,646, doi:10.1029/97JC0048
- Flocco, D., and D. L. Feltham, 2007. A continuum model of melt pond evolution on Arctic sea ice. *Journal of Geophysical Research*, doi: 10.1029/2006JC003836.
- Flocco, D., D. L. Feltham, and A. K. Turner, 2010. Incorporation of a physically based melt pond scheme into the sea ice component of a climate model. *Journal of Geophysical Research*, doi: 10.1029/2009JC005568.
- Hibler III, W., 1979. A dynamic thermodynamic sea ice model, *Journal of Physical Oceanography*, 9(4), 815–846, doi:10.1175/1520-0485.
- Holland, M. M., 2003. An improved single-column model representation of ocean mixing associated with summertime leads: Results from a SHEBA case study. *Journal of Geophysical Research: Oceans*, 108(C4).
- Holland, M. M., D. A. Bailey, B. P. Briegleb, B. Light, and E. Hunke, 2012. Improved sea ice shortwave radiation physics in CCSM4: The impact of melt ponds and aerosols on Arctic sea ice. *Journal of Climate*, doi: 10.1175/JCLI-D-11-00078.1.

Hunke and Lipscomb, 2010. CICE: the Los Alamos Sea Ice Model, Documentation and Software, Version 4.1. Los Alamos National Laboratory Tech. Rep. LA-CC-06-012.

Massonnet, F., T. Fichefet, H. Goosse, M. Vancoppenolle, P. Mathiot, and C. König Beatty, 2011. On the influence of model physics on simulations of Arctic and Antarctic sea ice. *The Cryosphere*, doi: 10.5194/tc-5-687-2011.

Massonnet, F., Barthélemy, A., Worou, K., Fichefet, T., Vancoppenolle, M., Rousset, C., and Moreno-Chamarro, E.: On the discretization of the ice thickness distribution in the NEMO3.6-LIM3 global ocean–sea ice model, *Geosci. Model Dev. Discuss.* <https://doi.org/10.5194/gmd-2019-16>, in review, 2019.

Rayner, N. A., Parker, D. E., Horton, E. B., Folland, C. K., Alexander, L. V., Rowell, D. P., Kent, E. C., Kaplan, A., 2003. Global analyses of sea surface temperature, sea ice, and night marine air temperature since the late nineteenth century *J. Geophys. Res.* Vol. 108, No. D14, 4407 10.1029/2002JD002670

Rousset, C., Vancoppenolle, M., Madec, G., Fichefet, T., Flavoni, S., Barthélemy, A., Benshila, R., Chanut, J., Levy, C., Masson, S., and F. Vivier, 2015. The Louvain-La-Neuve sea ice model LIM3.6: global and regional capabilities. *Geoscientific Model Development*, 8, 2991–3005, <https://doi.org/10.5194/gmd-8-2991-2015>

Schweiger, A., Lindsay, R., Zhang, J., Steele, M., Stern, H., and R. Kwok, 2011. Uncertainty in modeled Arctic sea ice volume, *J. Geophys. Res.*, 116, C00D06, <https://doi.org/10.1029/2011JC007084>

Shine, K. P., and A. Henderson-Sellers, 1985. The sensitivity of a thermodynamic sea ice model to changes in surface albedo parameterization. *Journal of Geophysical Research*, 90(D1): 2243-2250.

Thorndike, A. S., Rothrock, D. A., Maykut, G. A., and R. Colony, 1975. The thickness distribution of sea ice. *Journal of Geophysical Research*, 80(33), 4501–4513.

Titchner, H. A., and N. A. Rayner, 2014. The Met Office Hadley Centre sea ice and sea surface temperature data set, version 2: 1. Sea ice concentrations. *Journal of Geophysical Research: Atmospheres*, 119(6), 2864-2889.

Tsamados, M., Feltham, D. L., and A. V. Wilchinsky, 2013. Impact of a new anisotropic rheology on simulations of Arctic sea ice, *J. Geophys. Res. Oceans*, 118, 91–107.

Wilchinsky, A., and D. Feltham, 2006. Modelling the rheology of sea ice as a collection of diamond-shaped floes, *Journal of Non-Newtonian Fluid Mechanics*, 138(1), 22–32.

Zhang, J. L. and D. A. Rothrock, 2003. Modeling global sea ice with a thickness and enthalpy distribution model in generalized curvilinear coordinates, *Mon. Weather Rev.*, 131, 845-861.

#### **4. Lessons Learnt**

##### **Positive lessons:**

Some key results related to the impact of new developments on Arctic sea ice properties have been found. For example, introducing a more realistic melt pond scheme properly contributes to reduce the Arctic sea ice concentration and extent, and affect the feedback with the atmospheric component.

The WP3c activities exemplify well that joint efforts between two or more institutions can benefit research. In this particular case, it has allowed exploring different aspects of the same climate modelling feature (e.g. ice thickness distribution and melt ponds), with complementary analysis that have helped investigate in detail its impact on the sea ice.

##### **Negative lessons:**

The diversity of climate models and their component is an added value in climate studies, but has been somehow a limiting factor in this study to carry out a multi-model analysis and provide more robust assessments.

Increasing resolution in the ocean or atmospheric component does not systematically improve the results. In these particular sensitivity experiments, the updated sea ice model can improve some key processes and worsen other processes at high resolution, compared to the standard resolution.

#### **5. Links Built**

The simulations performed in this WP and the analyses presented in this report establish a direct link with WP1, e.g. the clustering algorithm used for the ITD analysis has been made available to all projects partners on Jasmin and has been described in the D1.2. It also has strong links with WP2, as the effect of resolution is analyzed with the different developments. Part of the work on ITD presented here stems from a collaboration between the UCLouvain and the BSC; it will further contribute to the H2020 project APPLICATE. Work on the implementation and analysis of melt-pond parameterizations in EC-Earth is a joint collaboration between UCLouvain, SMHI and BSC.